Disentangling the chemistry and transport impacts of the Quasi-Biennial Oscillation on stratospheric ozone

Jinbo Xie[1], Qi Tang[1], Michael Prather[2], Jadwiga Richter[3], Shixuan Zhang[4]

[1]Lawrence Livermore National Laboratory, Livermore, CA, USA

[2]Department of Earth System Science, University of California, Irvine, CA, USA

[3]National Center for Atmospheric Research, Boulder, CO, USA

[4]Pacific Northwest National Laboratory, Richmond, WA, USA

Correspondence to: Jinbo Xie (xie7@llnl.gov), now at Princeton University (jinbo.xie@princeton.edu)

Abstract

The quasi-biennial oscillation (QBO) in tropical winds perturbs stratospheric ozone throughout much of the atmosphere via changes in transport of ozone and other trace gases and via temperature changes, all of which alter ozone chemistry. Here we examine these changes using the Department of Energy's Energy Exascale Earth System Model version 2 (E3SMv2) with linearized stratospheric ozone chemistry. E3SM produces a natural QBO cycle in winds, temperature, and ozone. Our analysis identifies climatological QBO patterns of ozone for the period 1979-2020 using both nonlinear principal component analysis and monthly composites centered on the QBO phase transition month. As a free-running climate model, E3SM's QBO does not synchronize with the observed QBO, but it does match the climatological phasing of the observed patterns. With an offline version of our stratospheric chemistry module we calculate the local steady-state response of tropical ozone to the modeled changes temperature, chemical species, and overhead ozone column, and develop new diagnostics for QBO studies with interactive chemistry. Consistent with previous studies, we find clear demarcations with pressure. Ozone perturbations in the upper stratosphere (< 6 hPa) are predicted by the temperature changes; those between 6-hPa to 20-hPa are predicted by NO_y changes; and those in the lower stratosphere show no temperature or NO_y response and are presumably driven by circulation changes. Diagnostics that separate chemistry vs. transport driven changes in ozone provide insight into model differences in simulating the QBO.

1. Introduction

The Quasi-Biennial Oscillation (QBO) is the principal mode of dynamical variability in the tropical stratosphere, with impact on the circulation and greenhouse gases that extends from the tropical stratosphere into the troposphere. It is the key source of interannual variability in the overall chemical composition of the stratosphere (Randel et al., 1998; Shuckburgh et al. 2001; Park et al. 2017), manifest primarily through ozone (Reed 1964; Bowman, 1989; Wang et al., 2022).

The QBO affects ozone through both transport and chemical processes (Reed, 1964; Holton et al., 1989; Gray and Dunkerton, 1990; Chipperfield and Gray, 1992; Chipperfield et al., 1994, Politowicz and Hitchman, 1997; Jones et al., 1998; Baldwin et al., 2001). In the lower stratosphere where the ozone chemistry is slow, the alternate change of QBO phase speeds up and slows down the vertical ascent in the tropics that pushes the ozone profile up and down; in the middle and upper stratosphere, the ozone chemistry is fast and a chemical steady-state is maintained in spite of the transport. In this upper region the changes in vertical transport of trace gases like the total reactive nitrogen reservoir NO_y and the QBO dynamics-driven changes in temperature may also alter the ozone chemistry and produce new steady state values.

Disentangling the causes of QBO-ozone variability is useful for attributing ozone variability and understanding model-to-model differences in the QBO-ozone response that contributes to improved ozone and climate projections. For example, the impact of the ozone depleting substances may be underestimated if chemistry-driven ozone is mis-interpreted as transport-driven ozone, leading to potential bias in ozone projection and associated radiation calculation. However, challenges in attributing QBO-ozone variability remain due to co-dependence of temperature and transport (Baldwin et al, 2001), and model limitations in simulating a free-running QBO variability (Richter et al., 2020) including phase asymmetry (Scaife et al., 2014). The number of models with a naturally generated free-running QBO was 0 in the third Coupled Model Intercomparison Project (CMIP3); it rose to 5 in CMIP5 and to 15 in CMIP6 (Richter et al., 2020). Still, the amplitude and periods in these models often fail to match the observed pattern. In the current Chemistry–Climate Model Initiative (CCMI), many CCMs forced a QBO signal by nudging the equatorial zonal wind (Morgenstern et al., 2017). Nudging of the winds is inherently unphysical and produces an anomalous BDC not found in the free-running versions of the same CCMs (Orbe et al., 2020). The World Climate Research Project (WCRP) Atmospheric

Processes And their Role in Climate (APARC) started an QBO initiative (QBOi) in 2015 to improve CCM simulation of tropical variability (Butchart et al., 2018), and here we build on those experiments.

In this study, we use the interactive stratospheric chemistry module in E3SM (Linoz: Mclinden et al., 2000; Hsu and Prather, 2009) as an off-line model to calculate the photochemical steady-state value of ozone in response the local chemical composition, the temperature and the overhead column of ozone that determine photolysis rates. The Linoz code is based on tabulated linearization of the net chemical production of ozone and thus steady-state ozone can be derived from linear algebra. The determination of transport-driven ozone is then based on the difference of E3SM modeled ozone from the steady-state ozone. We also develop a new index of the QBO phase from a nonlinear principal component analysis (NLPCA) of the tropical zonal winds. Compared with the standard linear PCA QBO index (Wallace et al., 1993), NLPCA retains the observed asymmetric pattern and provides a more consistent measure of the phase throughout the cycle. The phase-based composite diagrams are then created to investigate the temporal evolution of ozone patterns, both observed and modeled.

Our primary modeling tool is the Department of Energy (DOE) Energy Exascale Earth Model version 2 (E3SMv2, Golaz et al., 2022) with interactive stratospheric ozone (Linoz v2 and Linoz v3; McLinden et al., 2000; Hsu and Prather, 2009), and secondarily we examine some QBO experiments from the National Center for Atmospheric Research (NCAR) Community Earth System Model (CESM). We find that QBO cycles in ozone can be attributed to temperature perturbations in the upper stratosphere (above 6-hPa), transport of NO_y between 6-hPa to 20-hPa, and mostly to circulation changes in the lower stratosphere (below 20-hPa) over a wide range of latitudes. The observational data and ozone modeling are described in section 2. The NLPCA method is presented in section 3, followed by the description and use of the Linoz off-line chemistry model in section 4. The results are in section 5. The discussion and conclusion are in section 6.

2. Data and methods

2.1 CCM models

The primary model for this study is E3SMv2. E3SM's atmospheric component (EAMv2) is run here as a CCM with specified sea surface temperatures (SSTs) and has 72 vertical layers and a horizontal resolution of about 100 km. Following Richter et al. (2010), EAMv2 employs

gravity wave (GW) parameterizations that include orographic GWs (McFarlane, 1987), convective GWs (Beres et al., 2004), and GWs generated by frontal systems (Charron and Manzini, 2002). Tunable parameters in the orographic and frontal GW parameterizations remain the same as in EAMv1 (Xie et al., 2018; Rasch et al., 2019). The tunable parameters in convective GWs were explored to produce a more realistic QBO in EAMv2 with a period around 27 months, much closer to observations (28 months) as compared to 16 months in EAMv1 (Richter et al., 2019). Nevertheless, the modeled QBO remains weak in amplitude. Stratospheric ozone in E3SMv2 is calculated interactively through transport and the chemical Linoz module (McLinden et al., 2000; Hsu and Prather, 2009) that was updated from the E3SM O3v1 to O3v2 module (Tang et al., 2021). Linoz v2 data tables are used to calculate the 24-hour-average ozone tendency (i.e., net production minus loss) from an adopted climatological mean state for key species (CH_4, H_2O, and NOy, Cly, Bry) and first-order Taylor series expansions about the local ozone, temperature, and overhead ozone column (see Eq. (3) in Sect. 4.1). The data tables are generated for each year assuming key chemical species and families (CH_4, H_2O, and NOy, Cly, Bry) follow monthly zonal-mean climatologies that scale with the slowly varying changes in tropospheric mean abundance of their source gases (e.g., N_2O, CFCs, halons, CH_4, tropopause H_2O). The Linoz model produces a reasonable stratospheric ozone climatology, including seasonal and interannual variability and the Antarctic ozone hole (Tang et al., 2021; Ruiz and Prather, 2022). The tropospheric chemical package for E3SMv2 (chemUCI) was not used and the lower boundary for Linoz was set to 30 ppb. Thus, none of the ozone column variability arises from tropospheric ozone chemistry. E3SMv2 diagnostics on the tendency of tropospheric ozone calculate a geographically resolved stratosphere-troposphere exchange (STE) flux of ozone every time step (Hsu et al., 2005; Tang et al., 2013).

The secondary model for this study is CESM2 (Emmons et al., 2020), using a modified version of the community atmosphere model (CAM) with 83 vertical levels (Randall et al., 2023; Isla et al., 2024), which is run here as a CCM with specified sea surface temperatures (SSTs). CAM uses the finite-volume dynamical core with a nominal 1° horizontal resolution and with physics from the Whole Atmosphere Community Climate Model version 6 (WACCM6; Gettleman et al. 2019). The parameters for the convective GW momentum transport were tuned especially for this version to obtain a realistic, naturally generated QBO (Randall et al., 2023). The inline ozone calculation in CESM2 is replaced with a monthly mean 3D ozone climatology

specified from a previous WACCM simulation. This input ozone forcing is formed by merging WACCM simulations for historical (1850-2014, 3 members) and future period (2015-2100, 1 member). As the mean of free-running CCM simulations, this ozone input climatology does not have any significant QBO-like variability, and thus it cannot trigger a QBO in the CCM (Butchart et al., 2023).

Both models are run with tropical winds being nudged to the observations and hence the synchronicity of the QBO should be similar and we can compare directly with observations. With the CESM2 QBO simulation we must limit our analysis to examining the forced dynamical response (temperature, circulation), but with E3SM results we can to compare the modeled QBO-ozone interactions with observations.

2.2 Observed ozone and wind

For ozone, we derive the observed QBO signal from the monthly zonal mean total column ozone (TCO) using the Multi-Sensor Reanalysis version 2 data (MSRv2, R.J. van der A, et al. 2015). This latitude-by-month dataset initially covers the period 1979-2012 and later extended to 2020. For stratospheric profiles, we use the zonal monthly mean latitude-by-altitude from the Concentration Monthly Zonal Mean (CMZM) product (Sofieva et al., 2023). This altitude-by-month profile data covers the period 1985-2020. The vertical levels are converted to pressure levels inverting the pressure-altitude formula, $z^* = 16 \log_{10}(1000/P)$ km. We compared this ozone data with the overlapping period from the Microwave Limb Sounder (MLS) data (V5 Level 3: Schwartz et al., 2021) and found only small differences with regard to QBO patterns.

We use ERA5 data (wind, temperature, geopotential height) from the reanalysis produced by the European Center for Medium-Range Weather Forecast (ECMWF) Integrated Forecast System (Hersbach et al., 2020). The version we use has 137 hybrid sigma model levels from the surface to the model top at 0.01 hPa, and the horizontal resolution is about 31 km. We use monthly mean data for the period 1979–2020 to analyze the QBO-related dynamical changes, and 6-hourly ERA5 tropical zonal wind (15°N-15°S) to nudge model simulations mentioned below. We use the 5°S-5°N tropical average zonal wind from ERA5 and simulations to determinate the QBO phase index. The combined station zonal wind data from Freie University of Berlin (Naujokat, 1986) for the period of 1979-2020 is also used.

2.3 The QBOi simulations

We use two experiments from the protocol for phase-2 of the QBOi (Butchart et al., 2018; Bushell et al., 2020; Richter et al., 2020):

(1) Exp1-ObsQBO (nudged): the zonal wind in the tropical stratosphere is constrained to follow the observed QBO evolution by nudging it toward ERA5 reanalysis (Hitchcock et al. 2022). Thus, the stratospheric climate including temperature and circulation in the tropics is constrained.

(2) Exp1-AMIP (natural): the zonal wind in the tropical stratosphere evolves freely in each CCM being forced only by SSTs and trace-gas radiative forcing; there is no nudging. The SSTs are historical and include interannual variability, primarily El-Nino and Southern Oscillation (ENSO).

The nudging is applied to the zonal wind over the range 8 hPa-to-80 hPa and 15°S-to-15°N (Fig. S1, nudging coefficient shown is for E3SMv2, that for CESM2 is similar). There is a slight difference in how the models were nudged: E3SMv2 is nudged to the "full field" ERA5 wind field including the longitudinal variability, while CESM2 is nudged to the zonally-averaged ERA5 zonal wind field. The nudging relaxation timescale is 5 days. The current setup forces the models to match the tropical QBO dynamic variability while allowing other variabilities to evolve freely (e.g. semi-annual oscillation). For each experiment we produced 3 ensemble members, and the ensemble mean is used for analysis.

To better understand the QBO-chemistry interactions, we performed two additional nudged single-ensemble 1979-2020 runs with E3SMv2 using different chemical models: one with an expanded stratospheric chemistry Linoz-v3 (Hsu and Prather, 2010), which calculates NO_y-N_2O-CH_4-H_2O as prognostic tracers and includes their interactions with ozone; a second with fixed ozone climatology as prescribed for CESM2.

3. NLPCA analysis of QBO phase

To build a time-line composite picture of the QBO in any variable, we need to define a phase of each QBOs and align these phases over a 28-month period. Phase asymmetry and nonlinear features of the evolution of the QBO phase are found in many studies (Lindzen and Holton 1968; Holton and Lindzen, 1972; Giorgetta et al., 2002). The most obvious and sharply defined synchronization point is when the QBO west phase (QBOw, i.e. prevailing westerlies) transitions to the east phase (QBOe: prevailing easterlies) at some pressure level in the middle stratosphere (taken as 10 hPa here) (Naujokat et al., 1986; Pahlavan et al., 2021; Kang et al., 2022). The

QBOe phase is typically longer (e.g., Bushell et al., 2019) with wind speeds about twice as strong as that of the QBOw (Naujokat et al., 1986; Kang et al., 2022). The problem with defining the QBO phase (index) simply as the month-to-month difference relative to the synchronization point (e.g., Ruiz et al., 2021) is that the duration of different phases varies across successive QBOs.

Previous use of PCA-derived QBO indices (Wallace et al., 1993) did not allow for this asymmetric and nonlinear behavior. Lu et al. (2009) noted that the reconstructed wind series from the PCA looked more sinusoidal in time than the actual winds, and thus the asymmetries between phases did not show up in the PCA-based indices. To address these issues, we use an NLPCA method that utilizes hierarchical-type neural network with an auto-associative architecture (Scholz et al. 2002). It is a nonlinear generalization of the standard PCA from straight lines to curves in the original data space, and natural extension to the PCA method by enforcing the nonlinear components to the same hierarchical order as in the standard PCA (Scholz et al., 2002). The NLPCA model described here has 5 layers with 3 hidden layers of neurons. The layers of the neural-network for NLPCA are in the sequence of input-encoding-bottleneck-decoding-output with the structure of n-(2k+2)-k-(2k+2)-n, where the n refers to dimension of input/output dataset and k is the number of dimensions for bottleneck layer. To achieve robustness, the NLPCA is applied to the tropical zonal wind data (5°S-5°N, 10-hPa to 70-hPa) for a set of k varying from 2 to 5, with 100 runs (different in random initialization weights) for each k. The optimal number of k is set as 5 as it gives the lowest root-mean-square-error between the input and output. The comparison of QBO phase angles and QBO transition points are shown in Fig. S2a and S2b. It is shown that the first and second principal components (PC1 and PC2) of the NLPCA account for approximately 90% of the whole variance (Figs. S2c and S2d).

Following previous studies (Wallace et al., 1993; Hamilton and Hsieh, 2002; Lu et al., 2009), the QBO phase index ψ is calculated using PC1 and PC2 as follows:

$$\psi = arctan\,(v/u) \quad (-\pi \le \psi \le \pi\,), \quad (1)$$

where u and v are the time series of the PC1 and PC2, respectively. The positive/negative phase angle index ψ corresponds to QBOw/QBOe.

We compare the reconstructed zonal wind anomalies using NLPCA and PCA (Wallace et al., 1993) with the QBO cycle in the observation (Fig. 1). It is shown that the observed QBO

transition corresponds to an abrupt downward propagation in QBOw and a slower downward transition in QBOe (indicated by clustering points in B to C to A on black triangular shape in Fig. 1a). The NLPCA captures large part of this sharp transition in QBOw while PCA underestimates it (indicated by points near C in Fig. 1a). This difference is also clearly shown in a typical QBO cycle of 1970. 9 – 1972.3 (Figs. 1b, 1c, and 1d, black arrow-sticks exhibits the downward propagation in QBOw) and the time series of NLPCA/PCA QBO phase (index) (Fig. S2).

While the NLPCA-derived QBO index is more realistic in following the atmospheric changes, it is impractical to map the NLPCA phases onto the monthly-mean model diagnostics. Thus, our QBO composites use simple monthly time steps about our best synchronization point, which from the NLPCA analysis we take to be at the transition when phase angle index ψ crosses 0 with negative values before and positive values after it (from QBO easterly to QBO westerly phase). It is demonstrated that comparing to QBO composites produced using the PCA-derived QBO index, those that produced using the NLPCA-derived index show a shifted QBO synchronization month (Fig. S2b). This results in larger contrast in observed tropical zonal wind anomalies between QBOw/QBOe (Figs. S3a and S3b) that is consistent with those described in previous literatures (Hamilton and Hsieh, 2002; Lu et al., 2009). This larger contrast between NLPCA and PCA in zonal wind anomalies is correspondent with the larger contrast in that of the total column ozone anomalies (Figs. S3c and S3d).

4. Linoz calculation of the steady-state ozone

To examine the ozone response to the QBO we use both Linoz v2 and v3 models. For Linoz v2 the steady-state ozone is derived from Eq. 4 of McLinden et al. (2000). The photochemical steady-state ozone mole fraction f_{ss} (parts per million, moles per mole of dry air) is expressed as follows:

$$f^{ss} = f^{o} + [\,(P-L)^{o} + \frac{\partial(P-L)}{\partial T}|^{o}\,(T-T^{o}) + \frac{\partial(P-L)}{\partial C_{O_3}}|^{o}(C_{O_3} - C^{o}_{O_3})\,]\tau, \qquad (2)$$

This is derived by setting $\frac{d(P-L)}{dt} = 0$ for Eq. 1 in McLinden et al., (2000). The values f^{o}, T^{o}, and $C^{o}_{O_3}$ are the climatological values of local ozone, temperature, and overhead column ozone tables used to calculate the Linoz tendencies. $(P–L)_o$ is the ozone net production minus loss tendency and the partial derivatives are the sensitivity of the net production to temperature and overhead column ozone.

A major assumption of Linoz v2 here is that the key chemical families (NO_y, Cl_y, Br_y) and long-lived reactive gases (N_2O, CH_4, H_2O) do not change from their climatological values used to generate the tables (Hsu and Prather, 2009). This steady-state calculation ignores transport tendencies and thus will be apply only where the photochemistry is rapid, i.e., $\tau = -[\frac{\partial(P-L)}{\partial f}|_o]^{-1} < 100$ days. Fig. 2 shows this Linoz v2 steady-state calculation (f_{SS}, T, τ) for January and July using ERA5 monthly mean temperature.

An alternative version (Linoz v3) of the steady state ozone derived from Hsu and Prather (2010) is expressed as follows:

$$f_{ss} = f_o + [(P-L)_o + \frac{\partial(P-L)}{\partial T}|_o (T-T_o) + \frac{\partial(P-L)}{\partial C_{O_3}}|_o (C_{O_3} - C^o_{O_3}) + \sum_{j=1}^{j=5} \frac{\partial(P-L)}{\partial f_j}|_o (f_j - f_j^o)]\tau, \quad (3)$$

This is similar as equation 2, except adds the contribution from sources of f_{N2O}, f_{NOy}, f_{CH4}, f_{H2O}. This may be used to provide a more precise diagnosis of the SSO from those models that have these output of chemistry species in addition to the temperature profile.

5. Impact of QBO on circulation and stratospheric ozone

Nudging the tropical zonal wind creates QBO-driven perturbations to the temperature and residual circulation that we can diagnose in both the E3SMv2 and CESM2 runs and compare with observations. For E3SMv2 with interactive ozone we are able to see the changes in ozone. This also applies to the simulations with an internally generated QBO.

We create a similar composite of the QBO cycle using E3SMv2/CESM2 following Ruiz et al., (2021) to see the full QBO cycle influence on stratospheric ozone. The time-composite is created for each month starting 14 months prior and extending to 14 months after the QBO transition for 1979-2020. The center is when the NLPCA-derived QBO phase angle index (see section 3) shifts from negative to positive (QBOe -> QBOw). We create composites for circulation (zonal wind, temperature and residual circulation) and chemistry tracers (total column ozone (TCO), ozone concentration, NO_y) as a function of QBO phase. For TCO, we calculate the zonal-mean averages to produce the global map of composite; for all other fields, we process the tropical (15°S-15°N) and extratropical (30°S-60°S/30°N-60°N) vertical profile of regional average using latitudinal weight to produce the composites. The CESM2 ozone composite is not shown since its ozone is prescribed.

In the following sections, we first analyze the impact of nudged QBO on circulation in E3SM and CESM in section 5.1. We then analyze its impact on global TCO and tropical/extratropical

ozone in section 5.2 and 5.3. The chemistry and transport impact of QBO are further analyzed using the steady-state ozone metric in section 5.4. The overall performances of the models are summarized in section 5.5.

5.1 Impact of QBO on circulation

In this section, we examine the impact of nudged QBO on circulation in both E3SMv2 and CESM2. We first analyze its impact on zonal wind and subsequently on temperature and residual circulation (e.g. $\underline{w}^*$, which characterizes the transport impact of the Brewer-Dobson Circulation).

Through nudging, the anomalous tropical zonal wind (15°S-15°N) in both nudged E3SMv2 and CESM2 simulations exhibit a similar negative-positive-negative pattern to that of ERA5 from QBOe to QBOw (Figure 3). In terms of the magnitude, E3SMv2's positive-negative pattern above 6-hPa is minorly stronger than that of ERA5 and CESM2. Despite this minor difference, both models overall reproduce the QBO signal in the tropics nudging regions. Correspondent to the zonal wind change, the tropical temperature in both models exhibit a negative-positive-negative-positive pattern like that of ERA5 (Figs. 4a-c). Alongside is the residual vertical transport $\underline{w}^*$ that exhibits a positive-negative-positive-negative pattern, like that of ERA5 (Figs. 4d-f). Studies have documented the QBOe tends to relate to cooling and upward advection while QBOw relates to warming and downward advection (Baldwin et al., 2001). The tropical temperature and $\underline{w}^*$ results shown are thus in-phase with zonal wind change in both models.

In the extratropic region (30°N-60°N/30°S-60°S), the results for the zonal wind are noisier (Fig. S4). The ERA5 results exhibit scattered signals of zonal wind changes for both hemispheres (Fig. S4a). The two models exhibit noisy results like that of ERA5, with CESM2 closer to ERA5. This is expected since the extratropics are more likely to be affected by dynamic noise from the polar regions. Unlike that of the zonal wind, the temperature and residual vertical transport $\underline{w}^*$ results are smoother for both observation and nudged simulations. It is shown that ERA5 exhibits about two cycles of positive-negative phase change for temperature (Figure 5a and 5d) and negative-positive phase change for $\underline{w}^*$ (Figs. 6a and 6d) from QBOe to QBOw, although southern hemisphere is noisier than northern hemisphere. Both models seem to have better accordance with ERA5 in the northern hemisphere (Figs. 5b, 5c and Figs. 6b, 6c), while E3SMv2 performs better than CESM2 in the southern hemisphere (Figs. 5e, 5f and Figs. 6e, 6f). Studies have documented that the QBO signal in the extratropics temperature and vertical advection are

306 at about 180° phase change relative to the tropical QBO signal (Baldwin et al., 2001). The results
307 shown here is in-phase with our nudged QBO signal in the tropics. Overall, the two models show
308 some signals of QBO-related signals outside of the regions of nudging on temperature and $\underline{w}^*$,
309 exhibiting the "spill-over" effect of QBO nudging.
310 To sum up, nudging creates more realistic QBO signal in both E3SMv2 and CESM2
311 especially in the tropical region. Outside of the nudging region, the "spill-over" effect of the
312 nudged QBO is seen mostly on temperature and $\underline{w}^*$ but less on the noisier zonal wind.

313 ## 5.2 Impact of QBO on global TCO

314 In this section, we examine the impact of QBO on ozone using TCO observations (MSRv2)
315 and E3SMv2 model simulations. The TCO composites from the E3SMv2 nudged simulation is
316 compared in Fig. 7. It is shown that the anomalous MSRv2 TCO exhibits a significant shift of
317 tripole pattern from QBOe to QBOw (Fig. 7a). The TCO pattern exhibits tri-pole pattern of
318 anomalous low in the tropics and high in the extratropics during QBOe that gradually transits to
319 tri-pole pattern of anomalous high in the tropics and low in the extratropic during QBOw. The
320 magnitude of the negative in QBOe (5 DU) is lower than the positive pattern (12 DU) in QBOw
321 in the tropics, indicating asymmetric phase response of TCO to QBO in the tropics. The E3SMv2
322 nudged simulation is like MSRv2 in that it captures most of the tripole patterns in both phases
323 with similar amplitudes (Fig. 7b), indicating the impact of nudged QBO on TCO is close to what
324 observed. It is shown that the internally generated QBO variability in E3SMv2 natural (Fig. S5a)
325 only partly exhibits the patterns of MSRv2 with weaker amplitude (nearly eight times weaker).
326 This indicates that nudging the tropical zonal wind contributes to the modulation and
327 enhancement of this "QBO-driven" TCO variability in E3SMv2.
328 Overall, the nudged E3SMv2 simulations show "QBO-driven" TCO variability in accordance
329 to observation that is partly present in E3SMv2 natural simulations and enhanced by QBO
330 nudging.

331 ## 5.3 Impact of QBO on tropical/extratropical stratospheric ozone

332 In this section, we analyze the impact of QBO on tropical (15°S-15°N) and extratropics
333 (30°S-60°S/30°N-60°N) stratospheric ozone concentration. The composites of ozone vertical
334 profile (1-hpa to 100-hPa) from E3SMv2 nudged and E3SMv2 Linoz-v3 nudged simulations are
335 compared with the CMZM satellite data (Fig. 8).

In the tropics, it is shown that the CMZM satellite ozone exhibits a double-peak vertical structure with large ozone variations between 1~20-hPa and 20~100-hPa (Fig. 8a). Both peaks shift in a sequence of negative-positive-negative from QBOe to QBOw, and the amplitude of the upper peak is smaller than that of the lower peak (Fig. 8a). The E3SMv2 nudged simulation captures most of the double-peak structure (Fig. 8b) with minor exceptions – the anomalous high ozone in CMZM from month -14 to month -8 around 10-hPa and the anomalous low around 10-hPa from month -2 to month 2 is missed. Studies have documented NO_y variations as the primary drivers of ozone QBO changes around this range (Chipperfield et al., 1994; Tian et al., 2006). Since E3SMv2 nudged uses the Linoz-v2 which the chemistry species such as CH_4 or NO_y remain constant, the deficiency may be due to uncertainty in these chemistry species. To test this assumption, we also compared the E3SMv2 Linoz-v3 nudged simulation (with chemistry impact of NO_y-N_2O-CH_4-H_2O) with CMZM (Figure 8c). It is shown that the E3SMv2 Linoz-v3 nudged simulation captures both missing parts in E3SMv2 nudged, indicating that this missing chemistry may be responsible for this deficiency. The E3SMv2 natural simulations, on the other hand, show similar double-peaked patterns but with smaller amplitude (3 times weaker) and shorter period (Fig. S5b). This may be because the period of internally generated QBO in E3SMv2 is ~21 years (Golaz et al., 2022). Overall, the E3SMv2 nudged simulation modifies the period and enhances the QBO response in tropical ozone that is mostly consistent with the CMZM weaker above 20-hPa and stronger below 20-hPa with deficiency around 10-hPa. This deficiency is rectified by improved representation of NO_y-N_2O-CH_4-H_2O chemistry in E3SMv2 Linoz-v3 nudged simulation.

This analysis is extended to the E3SMv2 nudged simulations in the extratropical region in both hemispheres (30°N-60°N/30°S-60°S). Since the nudging is imposed only in the tropical regions, we can further examine the impact of nudged QBO in the extratropics where it is free running. Fig. 9 shows pressure-time cross-section of the extratropical (30°N-60°N/30°S-60°S) ozone concentration as a function of QBO phase for CMZM satellite ozone, E3SMv2 nudged and E3SMv2 Linoz-v3 nudged simulations. Unlike that of the tropics, the extratropical ozone for CMZM is noisier despite an overall in-phase change with QBO (Figs. 9a and 9d). The exception is in the northern hemisphere where the QBOw exhibits an extra phase change to positive (Fig. 9a). It is shown that nudged E3SMv2 simulations follow the similar positive-negative ozone phase shift in both hemispheres (Figs. 9b and 9e) without the noisy phase change in northern

hemisphere. In terms of the amplitude, the QBOw is similar for both hemisphere but weaker than CMZM in QBOe. E3SMv2 Linoz-v3 nudged simulation tends to be similar to that of E3SMv2 nudged simulation, except the amplitude in QBOw is stronger (Figs. 9c and 9f). Overall, the E3SMv2 nudged and E3SMv2 Linoz-v3 nudged partly capture in-shift with QBO in extratropical ozone in both hemispheres despite amplitude difference.

5.4 Separating the chemistry and transport impact of QBO on ozone using Linoz steady-state ozone

In this section, we utilize the Linoz steady-state ozone (equation 2 and 3, see section 4 for detail) introduced in section 4 to separate the chemistry and transport impact of QBO on ozone. As a coupled system, the QBO chemical and transport impacts on ozone are intertwined, making it difficult to diagnose which QBO impact is more prominent to the ozone differences between model and observation or among different models. Here we try to quantitatively separate these two terms with this new diagnostic tool, recognizing their time scale differences. We first derive the Linoz-v2 steady state ozone (equation 2) for E3SMv2 nudged and CESM2 nudged simulations (Fig. 10). Although ozone is prescribed in CESM2, the steady state ozone for CESM2 shown here is the "would-be" temperature-ozone if CESM2 were to implement Linoz v2 as its ozone module. To further analyze the impact of temperature and different chemistry species (NO_y, N_2O, H_2O, CH_4) in ozone simulation, the steady state ozone using temperature only (equation 2) and using temperature plus chemistry species (equation 3) are derived for E3SMv2 Linoz-v3 nudged (Fig. 11).

In the tropics (15°S-15°N), the Linoz-v2 steady state ozone from E3SMv2 and CESM2 nudged exhibit an apparent negative-positive-negative pattern above 20-hPa (Figs. 10a and 10d). These correspond to the temperature patterns above 20-hPa shown in the previous section (Figs. 4b and 4c). This pattern in E3SMv2v is like that of the E3SMv2 ozone pattern above 20-hPa (Fig. 8b), indicating a temperature impact mostly above 20-hPa. Below 20-hPa, the prognostic ozone in E3SMv2 correspond to the alternating $\underline{w}^*$ shift patterns (Fig. 4e). The residual meridional circulation shows a weaker magnitude below 20-hPa and is thus less likely to play a major role in ozone change (Fig. S6). This and the no response in steady state ozone indicates the prognostic ozone below 20-hPa in E3SMv2 is transport-driven. Like that of the analysis in the tropics, the temperature impact in the extratropics (30°N-60°N/30°S-60°S) is stronger above 20-hPa for both E3SMv2 (Figs. 10b and 10c) and CESM2 (Figs. 10e and 10f) nudged simulations.

The difference is that the Southern Hemisphere (30°S-60°S) is overall noisier than that of the northern hemisphere (30°N-60°N). This noisier southern hemisphere steady state ozone above 20-hPa in the nudged simulations correspond to the noisier temperature for the two models (Figs. 5c and 5f), which may be largely affected by stronger and noisier southern polar vortex (Fig. S7) as also documented by other studies (Ribera et al., 2004). The intrusion of the polar vortex via events like stratospheric sudden warming (Butler et al., 2017) may have an impact on the QBO-ozone relationship in the extratropics. Below 20-hPa, the E3SMv2 nudged ozone corresponds to the $\underline{w}^*$ (Fig. 10b and 10e), indicating it's transport-driven. Overall, with the application of Linoz-v2 on E3SMv2 nudged simulation, we can partly separate the temperature-driven and transport-driven QBO-ozone around the boundary of 20-hPa in both tropics and extratropics. The limit in this application lies in the uncertainty in exclusion of chemistry transport such as NOy in the simulations.

To test the sensitivity of the results to the chemistry variations, we further applied Linoz-v2 steady-state ozone (equation 2, temperature-only) and Linoz-v3 steady-state ozone (equation 3, temperature plus chemistry) to E3SMv2 Linoz-v3 nudged simulation (Fig. 11). It is shown that the steady-state ozone including temperature plus chemistry variation show better accordance with observed ozone than including temperature only especially in both the tropics (Figs. 8a, 11a, and 11d) and the extratropics (Figs. 9a, 9b, 11c, 11d, 11e, and 11f). This better accordance is especially apparent between 6-hPa to 20-hPa and in good accordance with the NO_y change (Fig. 12), indicating the impact of chemistry variation within this height. To further examine the variable responsible for the change, the single specie sensitivity test is also done (not shown). It is shown that including temperature plus NO_y variation can reproduce the patterns in Figs. 11a-c. This indicates the NO_y variation an important driver around 6-hPa to 20-hPa in QBO-ozone, in accordance with the previous studies (Chipperfield et al., 1994; Tian et al., 2006).

The results here indicate demarcations of QBO-induced ozone at 6-hPa and 20-hPa. These demarcations of the QBO-induced ozone at 6-hPa and 20-hPa may be due to the separation of ozone lifetime below/above 20-hPa (Reed et al., 1964) and NO_y variation (Chipperfield et al., 1994; Tian et al., 2006). The ozone lifetime is relatively long compared with the dynamical process below this level while shortened considerably above it. The temperature affects ozone above 20-hPa (especially above 6-hPa) through ozone destruction – colder/warmer anomalies slow/accelerate ozone destruction, leading to correspondent ozone increase/decrease (Wang et

al., 2022); the transport effect of QBO-related wind modulates the temperature through thermal wind balance enhancing/lessening the upward motion in the tropics (Plumb and Bell, 1982; Baldwin et al., 2001; Ribera et al., 2004; Punge et al., 2009). In the extratropics, the process is similar except controlled by the return arm of QBO-induced circulation that is in 180° phase reversal with the tropics (Baldwin et al., 2001). This explains the apparent separation of transport- and chemistry-driven ozone changes above/below 20-hPa. Between 6-hPa to 20-hPa, QBO modulation of NO_y variation is shown to be an important contributor of the QBO-ozone cycle in addition to the temperature impact (Chipperfield et al., 1994). This explains the better reproduction of steady-state ozone above 20-hPa when including NO_y variation. Overall, the demarcations of QBO-induced ozone shown here can be overall explained by photochemical process above 6-hPa, NO_y variation between 6-hPa and 20-hPa, and circulation change in vertical advection below 20-hPa. It is also worth mentioning that the nudged CESM2 also produces similar temperature and $\underline{w}^*$. This indicates that nudged CESM2 may produce similar prognostic ozone if it were to implement Linoz as interactive ozone module.

5.5 Model performance in simulating QBO impact

In this sub-section, we examine the overall performance of E3SMv2 and CESM2 QBOi simulations in simulating the QBO-ozone relationship. We evaluate the pattern correlation and standard deviation of the area-weighted TCO pattern (60°S-60°N), vertically-weighted ozone concentration (15°S-15°N, 30°N-60°N, 30°S-60°S), zonal wind (15°S-15°N, 30°N-60°N, 30°S-60°S), temperature (15°S-15°N, 30°N-60°N, 30°S-60°S), and $\underline{w}^*$ (15°S-15°N, 30°N-60°N, 30°S-60°S). For ozone, only E3SMv2 results are shown since CESM2 has fixed ozone. The results are summarized in a Taylor diagram shown in Fig. 13. The observed pattern is plotted at the (1,0) reference point.

In terms of ozone (Fig. 13a), there are remarkable differences between the simulations. Overall, the E3SMSv2 nudged simulations perform the best, with the pattern correlation of all four variables over 0.8 while other simulations are below 0.5. This indicates nudging realistic QBO variability may increase the model performance in simulating ozone. In the extratropics, the E3SMv2 nudged simulation has good pattern correlations, but the amplitude is off by over 1.5 times. The results for temperature, zonal wind and $\underline{w}^*$ are similar with ozone in the tropics (Figs. 13b, 13c, and 13d). What's different is in the extratropics — both nudged

E3SMv2/CESM2 temperature, zonal wind, and $\underline{w}^*$ show better performance in NH extratropics than in SH extratropics. This may be due to stronger polar vortices in SH and NH that disturb the QBO signal. Another difference is in the natural simulations – the tropical temperature (15°S-15°N) and zonal wind signals exhibit reasonable correlations of over 0.7 in zonal wind, over 0.5 in temperature. This indicates a discernable internally generated QBO signal in the E3SMv2/CESM2, although it's weaker and does not extend to the extratropics.

6. Discussion and Conclusion

6.1 Discussion

There are some interesting issues worth discussing in this section. Firstly, the use of the offline Linoz model provides an useful tool to diagnose the dynamic and chemical impact of QBO on ozone. The Linoz v2 SSO metric can be applied to all models with the with the minimum need of temperature profile only. One caveat of this approach is that current Linoz-v2 neglects the potential impact of cross-over chemical species such as the NO_y that has been shown to be an important driver for QBO-ozone change between 6-hPa to 20-hPa. Thus, it would be recommended to include at least the NO_y output by the CCMs for a more precise diagnostic between this height range. The tools shown here can be valuable to diagnose the uncertainty in the QBO-ozone relationship among difference models.

Another noteworthy issue is the nudging employed in the current study. Nudging has been adopted by models from different climate centers in the QBOi project to ensure the realistic simulation of QBO through constraining the tropical climate. The differences in the strategies of nudging in these models and their effects on the QBO climate are thus needed to be analyzed with care. Our study showed that the nudging overall constrains both E3SMv2 and CESM2 towards a realistic representation of QBO-associated temperature and residual circulation field outside of the nudged regions (15S-15N tropics). However, differences in the nudging strategies can play a role in the detailed features of the zonal wind and temperature simulated by two models. For example, the extratropical zonal wind and temperature in CESM2 showed more scattered features than those in E3SMv2 in our simulations. This may be partly because the full field nudging in E3SMv2 nudge all zonal wavenumbers. This may pose a stronger constraint on field than the zonal mean nudging in CESM2 that may nudge less field of high wavenumbers.

Lastly, the impact of ozone feedback on the climate in this study deems further attention. The two models compared here show overall similar QBO-signal with nudging despite have two different ozone modules – one interactive and another non-interactive. One may question what the results would be with the same modules under nudging. The sensitivity test of E3SMv2 fixed-ozone nudged simulation shows that with fixed-ozone, the temperature patterns are still retained although with an amplified magnitude in both the tropics and extratropics (Fig. S7). This indicates a strong nudging impact, and an overall damping effect of interactive ozone in E3SMv2.

6.2 Conclusion

In this study, we utilize the Linoz steady state ozone on nudged climate model simulations to separate the chemical and transport response of the QBO ozone impact. We derive a new QBO phase index using the NLPCA method and utilize this index to form QBO cycle composites to analyze QBO-ozone relationships in observation and simulations. By analyzing the simulations from two QBOi participant models (E3SMv2 and CESM2), we found that the nudged simulations can produce a reasonable QBO impact in the tropics and "spill-over" impact on fields like temperature and residual circulation in the extratropics to be in-phase with tropic QBO signal. The nudged E3SMv2 simulation captures the tripole composite pattern in the observed TCO. Nudging was also shown to improve the double-peaked vertical structure in observed ozone data between 1~20-hPa and 20~100-hPa over the tropics. In the extratropics outside of the nudging region, the nudged E3SMv2 simulated ozone tends to be overall in-phase with the observed but with magnitude difference, indicating the "spill-over" impact of nudged QBO signal.

Utilizing the Linoz steady-state ozone metric, we separated the chemical and transport response of ozone in E3SMv2 nudged to QBO. It is shown that these impacts have rather clear demarcations on both tropical and extratropical ozone response at 6-hPa and 20-hPa – chemistry impact correspondent to QBO-related temperature change dominates the response above 6-hPa linked to photochemical process, between 6-hPa to 20-hPa linked to NO_y variation, and transport impact related to QBO-related vertical advection dominates the response below 20-hPa. The results here are important for diagnosing model-model and model-observation differences in the QBO with free-running climate-change simulations, allowing us to separate chemical from circulation effects.

Stratospheric ozone is not only essential for protecting life on the Earth but also has important climate impacts. More and more studies reported the important role of ozone variations in modifying the stratospheric circulation and therefore influencing the surface climate

(e.g. Xie et al., 2020). Since the QBO has relatively high predictability, considering its impacts on stratospheric ozone and subsequent atmospheric circulations may help improve the predictions of surface weather and climate (e.g., Li et al., 2023).

Despite the above studies, however, there are still caveats. The current study makes use of only one model in QBOi that has an interactive ozone feature. More models may be used in the future to examine the QBO-ozone relationship. These are to be assessed in future studies.

Data availability

The satellite data from the Copernicus Climate Change Service can be accessed at (https://cds.climate.copernicus.eu/cdsapp#!/dataset/satellite-ozone-v1?tab=form). The ERA5 data can be accessed at (https://cds.climate.copernicus.eu/cdsapp#!/dataset/reanalysis-era5-complete?tab=overview). The ChemDyg diagnostics can be accessed at (https://doi.org/10.5281/zenodo.11166488).

Author contribution

J.X., Q.T. designed the research; J.X. performed the E3SM simulations and wrote the manuscript. J.R. provided the CESM2 simulation. Q. T. and M.P.'s supervised the research and helped interpreting the results. All authors contributed to the scientific discussion and paper revision.

Competing interests

The authors declare that they have no conflict of interest.

Acknowledgement

We thank the Copernicus Climate Change Service for providing the satellite data and ECMWF for the ERA5 data. We thank Isla Simpson for setting up the CESM2 QBOi simulations, and providing the Python script for generating the Transformed Eulerian Mean variables. We thank Sasha Glenville for transferring the CESM2 data. This research was supported as part of the E3SM project, funded by the U.S. Department of Energy, Office of Science, Office of Biological

and Environmental Research. Part of the work was supported by the LLNL LDRD project 22-ERD-008 titled “Multiscale Wildfire Simulation Framework and Remote Sensing”. E3SM simulations were performed on a high-performance computing cluster provided by the BER ESM program and operated by the Laboratory Computing Resource Center at Argonne National Laboratory. Additional post-processing and data archiving of production simulations used resources of the National Energy Research Scientific Computing Center (NERSC), a DOE Office of Science User Facility supported by the Office of Science of the U.S. Department of Energy under Contract No. DE-AC02-05CH11231. This work was performed under the auspices of the U.S. Department of Energy by Lawrence Livermore National Laboratory under contract DE-AC52-07NA27344. The IM release number is LLNL-JRNL-858987. This work was in part supported by the National Center for Atmospheric Research (NCAR), which is a major facility sponsored by the National Science Foundation (NSF) under Cooperative Agreement 1852977. Portions of this study were supported by the Regional and Global Model Analysis (RGMA) component of the Earth and Environmental System Modeling Program of the U.S. Department of Energy’s Office of Biological and Environmental Research (BER) via NSF Interagency Agreement 1844590.

Reference

Andrews, M. B., Knight, J. R., Scaife, A. A., et al.: Observed and Simulated Teleconnections Between the Stratospheric Quasi-Biennial Oscillation and Northern Hemisphere Winter Atmospheric Circulation, J. Geophys. Res., 124, 1219–1232, https://doi.org/10.1029/2018JD029368, 2019.

Andrews, D.G., J.R. Holton, and C.B. Leovy: Middle Atmosphere Dynamics. Academic Press, 489pp, 1987.

Anstey, J. A. and Shepherd, T. G.: High-latitude influence of the quasi-biennial oscillation, Q. J. Roy. Meteor. Soc., 140, 1–21, https://doi.org/10.1002/qj.2132, 2014.

Baldwin, M. P., Birner, T., Brasseur, G., et al.: 100 years of progress in understanding the stratosphere and mesosphere, Meteor. Mon.,59, 27.1–27.62, https://doi.org/10.1175/AMSMONOGRAPHSD-19-0003.1, 2019.

Baldwin, M. P., Gray, L. J., Dunkerton, T. J., et al., The quasi-biennial oscillation, Rev. Geophys., 39, 179–229, 2001.

Baldwin M. P., Tung KK., Extra-tropical QBO signals in angular momentum and wave forcing. Geophys. Res. Lett. 21: 2717–2720, 1994.

Beljaars, A. C. M., Brown, A. R., & Wood, N.: A new parameterization of turbulent orographic form drag. Quarterly Journal of the Royal Meteorological Society, 130, 1327–1347. https://doi.org/10.1256/qj.03.73, 2004.

Bowman, K. P.: Global patterns of the quasi-biennial oscillation in total ozone. *J. Atmos. Sci.,***46,** 3382–3343, 1989.

Brasseur, G., Hauglustaine, D., Walters, S., Rasch, P., Muller, J., Granier, C., & Tie, X: MOZART, a global chemical transport model for ozone and related chemical tracers 1. Model description. Journal of Geophysical Research-Atmospheres, 103(D21), 28,265–28,289. https://doi.org/10.1029/98JD02397, 1998.

Burkholder, J. B., Sander, S. P., Abbatt, J., Barker, J. R., Huie, R. E., Kolb, C. E., et al.: Chemical kinetics and photochemical data for use in atmospheric studies, evaluation no. 18, JPL Publication 15–10, Jet Propulsion Laboratory, Pasadena, CA. Retrieved from http://jpldataeval.jpl.nasa.gov, 2015.

Bushell, A. C., Anstey, J. A., Butchart, N., et al.:Evaluation of the quasi-biennial oscillation in global climate models for the SPARC QBO-initiative. *Quarterly Journal of the Royal Meteorological Society*, *148*(744), 1459-1489, 2020.

Butchart, N., Andrews, M. B., & Jones, C. D.: QBO phase synchronization in CMIP6 historical simulations attributed to ozone forcing. *Geophysical Research Letters*, 50, e2023GL104401. https://doi.org/10.1029/2023GL104401, 2023.

Butchart, N., Anstey, J. A., Hamilton, K., et al.: Overview of experiment design and comparison of models participating in phase 1 of the SPARC Quasi-Biennial Oscillation initiative (QBOi). *Geoscientific Model Development*, *11*(3), 1009-1032, 2018.

Butchart, N., Charlton-Perez, A. J., Cionni, I., et al.: Multimodel climate and variability of the stratosphere, J. Geophys. Res., 116, D05102, https://doi.org/10.1029/2010JD014995, 2011.

Butchart, N., Scaife, A.A., Austin, J., et al.: Quasi-biennial oscillation in ozone in a coupled chemistry-climate model. J. Geophys. Res.: Atmosphere 108 (D15), 4486, 2003.

Butler, A. H., Sjoberg, J. P., Seidel, D. J., Rosenlof, K. H.: A sudden stratospheric warming compendium, Earth System Science Data. 9 (1): 63–76. doi:10.5194/essd-9-63-2017.

608 Charron, M., and Manzini, E.: Gravity waves from fronts: Parameterization and middle
609 atmosphere response in a general circulation model. *Journal of the Atmospheric Sciences*,
610 59(5), 923– 941. https://doi.org/10.1175/1520-0469(2002)059<0923:gwffpa>2.0.co;2, 2002.
611 Chipperfield, M. P., & Gray, L. J. : Two-dimensional model studies of the interannual
612 variability of trace gases in the middle atmosphere. *Journal of Geophysical Research:*
613 *Atmospheres*, *97*(D5), 5963-5980, 1992.
614 Chipperfield, M. P., Gray, L. J., Kinnersley, J. S., Zawodny, J.: A two-dimensional model study
615 of the QBO signal in SAGE II NO2 and O3. *Geophysical research letters*, *21*(7), 589-592,
616 1994.
617 Coy, L., Wargan, K., Molod, A. M., et al.: Structure and dynamics of the quasi-biennial
618 oscillation in MERRA-2, J. Climate, 29, 5339–5354, 2016.
619 Danabasoglu, G., Lamarque, J.-F., Bacmeister, J. et al.: The Community Earth System Model
620 Version 2 (CESM2). Journal of Advances in Modeling Earth Systems,12, e2019MS001916.
621 https://doi.org/10.1029/2019MS001916, 2020.
622 Dunkerton, T. J.: The role of gravity waves in the quasi-biennial oscillation, J. Geophys. Res.,
623 102, 26,053-26,076, 1997.
624 Elsbury, D., Peings, Y., and Magnusdottir, G.:, Variation in the Holton-Tan effect by longitude,
625 Q. J. Roy. Meteor. Soc., 147,1767–1787, https://doi.org/10.1002/qj.3993, 2021.
626 Emmons, L. K., Schwantes, R. H., Orlando, J. J., et al.: The Chemistry Mechanism in the
627 Community Earth System Model version 2 (CESM2). Journal of Advances in Modeling Earth
628 Systems, 12, e2019MS001882. https://doi.org/10.1029/2019MS001882, 2020.
629 Emmons, L. K., Hauglustaine, D. A., Müller, J. F., Carroll, M. A., Brasseur, G. P., Brunner, D.,
630 et al.: Data composites of airborne observations of tropospheric ozone and its precursors.
631 Journal of Geophysical Research-Atmospheres, 105(D16), 20497–20538.
632 https://doi.org/10.1029/2000jd900232, 2000.
633 Garfinkel, C. I., Shaw, T. A., Hartmann, D. L., and Waugh, D.W.: Does the Holton-Tan
634 Mechanism Explain How the Quasi-Biennial Oscillation Modulates the Arctic Polar Vortex?, J.
635 Atmos. Sci., 69, 1713–1733, https://doi.org/10.1175/JAS-D-11-0209.1, 2012.
636 Gettelman, A., & Morrison, H.: Advanced two-moment bulk microphysics for global models.
637 Part I: Off-line tests and comparison with other schemes. Journal of Climate, 28, 1268–1287.
638 https://doi.org/10.1175/JCLI-D-14-00102.1, 2015.
639 Giorgetta, M. A., Manzini, E., and Roeckner, E.: Forcing of the quasi-biennial oscillation from
640 a broad spectrum of atmospheric waves. *Geophysical Research Letters*, *29*(8), 86-1, 2002.
641 Golaz, J.-C., Van Roekel, L. P., Zheng, X. et al. : The DOE E3SM Model version 2: Overview
642 of the physical model and initial model evaluation. Journal of Advances in Modeling Earth
643 Systems, 14, e2022MS003156. https://doi.org/10.1029/2022MS003156, 2022.
644 Golaz, J.-C., Caldwell, P. M., Van Roekel, L. P. et al.: The DOE E3SM coupled model version
645 1: Overview and evaluation at standard resolution. *Journal of Advances in Modeling Earth*
646 *Systems*, 11(7), 2089– 2129. https://doi.org/10.1029/2018MS001603, 2019.
647 Golaz, J.-C., Larson, V. E., & Cotton, W. R. A PDF-based model for boundary layer clouds.
648 Part I: Method and model description. Journal of the Atmospheric Sciences, 59, 3540–3551,
649 2002.
650 Gray, L. J., & Dunkerton, T. J.: The role of the seasonal cycle in the quasi-biennial oscillation
651 of ozone. *Journal of Atmospheric Sciences*, *47*(20), 2429-2452, 1990.

Hamilton, K., & Hsieh, W. W.: Representation of the quasi-biennial oscillation in the tropical stratospheric wind by nonlinear principal component analysis. *Journal of Geophysical Research: Atmospheres*, *107*(D15), ACL-3, 2002.
Hamilton, K. : Interhemispheric asymmetry and annual synchronization of the ozone quasi-biennial oscillation. *Journal of Atmospheric Sciences*, *46*(7), 1019-1025, 1989.
Hansen, F., Matthes, K., and Gray, L. J.: Sensitivity of stratospheric dynamics and chemistry to QBO nudging width in the chemistryclimate model WACCM, J. Geophys. Res., 118, 10464–10474, https://doi.org/10.1002/jgrd.50812, 2013.
Hasebe, F.: Quasi-biennial oscillations of ozone and diabatic circulation in the equatorial stratosphere, *J. Atmos. Sci.*, 51, 729–745, 1994.
Hersbach H, Bell B, Berrisford P, et al.: The ERA5 global reanalysis, *Q J R Meteorol Soc*. 2020; 146: 1999–2049. https://doi.org/10.1002/qj.3803, 2020,
Hitchcock, P., Butler, A., Charlton-Perez, A., et al.: Stratospheric Nudging And Predictable Surface Impacts (SNAPSI): a protocol for investigating the role of stratospheric polar vortex disturbances in subseasonal to seasonal forecasts. *Geoscientific Model Development*, *15*(13), 5073-5092, 2022.
Hitchman, M. H., and C. B. Leovy: Estimation of the Kelvin wave contribution to the semiannual oscillation, *J. Atmos. Sci.*, 45, 1462, 1988.
Holton, J. R. and Tan, H.-C.: The quasi-biennial oscillation in the Northern Hemisphere lower stratosphere, J. Meteor. Soc. Japan.,60, 140–148, 1982.
Holton, J. R. and Tan, H.-C.: The influence of the equatorial quasi-biennial oscillation on the global circulation at 50 mb, J. Atmos. Sci., 37, 2200–2208, 1980.
Holton, J. R.: Influence of the annual cycle in meridional transport on the quasi-biennial oscillation in total ozone. *Journal of Atmospheric Sciences*, *46*(10), 1434-1439, 1989.
Holton, J. R., and R. S. Lindzen: An updated theory for the quasi-biennial cycle of the tropical stratosphere, *J Atmos. Sci.*, 29, 1076, 1972.
Horowitz, L. W., Walters, S., Mauzerall, D. L., Emmons, L. K., Rasch, P. J., Granier, C., et al.: A global simulation of tropospheric ozone and related tracers: Description and evaluation of MOZART, version 2. Journal of Geophysical Research-Atmospheres, 108(D24), 4784. https://doi.org/10.1029/2002jd002853, 2003.
Hsu, J. and Prather, M. J.: Stratospheric variability and tropospheric ozone, J. Geophys. Res.-Atmos., 114, D06102, https://doi.org/10.1029/2008JD010942, 2009.
Hsu, J., and M. J. Prather: Global long-lived chemical modes excited in a 3-D chemistry transport model: Stratospheric N_2O, NO_y, O_3 and CH_4 chemistry, *Geophys. Res. Lett.*, 37, L07805, doi:10.1029/2009GL042243, 2010.
Hsu, J., M. J. Prather, and O. Wild: Diagnosing the stratosphere-to-troposphere flux of ozone in a chemistry transport model, J. Geophys.Res., 110, D19305, doi:10.1029/2005JD006045, 2005.
Isla et al.: Toward the vertical resolution of the next generation of the Community Atmosphere Model, To be submitted, 2024.
Jones, D. B., Schneider, H. R., & McElroy, M. B.: Effects of the quasi-biennial oscillation on the zonally averaged transport of tracers. *Journal of Geophysical Research: Atmospheres*, *103*(D10), 11235-11249, 1998.
Jucker, M., Reichler, T., & Waugh, D. W.: How frequent are Antarctic sudden stratospheric warmings in present and future climate?. *Geophysical Research Letters*, *48*(11), e2021GL093215, 2021.

Kang, M. J., Chun, H. Y., Son, S. W., et al.: Role of tropical lower stratosphere winds in quasi-biennial oscillation disruptions. *Science Advances*, *8*(27), eabm7229, 2022.
Kinnersley, J. S., and Tung, K. K.: Mechanisms for the extratropical QBO in circulation and ozone. *Journal of the atmospheric sciences*, *56*(12), 1942-1962, 1999.
Kinnison, D. E., Brasseur, G. P., Walters, S., Garcia, R. R., Marsh, D. R., Sassi, F., et al.: Sensitivity of chemical tracers to meteorological parameters in the MOZART-3 chemical transport model. Journal of Geophysical Research-Atmospheres, 112(D20), D20302. https://doi.org/10.1029/2006jd007879, 2007.
Lamarque, J. F., Emmons, L. K., Hess, P. G., Kinnison, D. E., Tilmes, S., Vitt, F., et al.: CAM-chem: Description and evaluation of interactive atmospheric chemistry in the Community Earth System Model. Geoscientific Model Development, 5(2), 369–411. https://doi.org/10.5194/gmd-5-369-2012, 2012.
Larson, V. E. : CLUBB-SILHS: A parameterization of subgrid variability in the atmosphere. arXiv:1711.03675v2 [physics.ao-ph], 2017.
Lawrence, B. N. : A gravity-wave induced quasi-biennial oscillation in a three-dimensional mechanistic model. *Quarterly Journal of the Royal Meteorological Society*, *127*(576), 2005-2021, 2001.
Lee, S., Shelow, D., Thompson, A.M., Miller, S.: QBO and ENSO variability in temperature and ozone from SHADOZ, 1998–2005. J. Geophys. Res.: Atmosphere 115 (D18105), 2010.
Lee, H.-H., Tang, Q., and Prather, M.: E3SM Chemistry Diagnostics Package (ChemDyg) Version 0.1.4, Geosci. Model Dev. Discuss. [preprint], https://doi.org/10.5194/gmd-2023-203, in review, 2024.
Leung, L. R., Bader, D. C., Taylor, M. A., and McCoy, R. B.: An introduction to the E3SM special collection: Goals, science drivers, development, and analysis. *Journal of Advances in Modeling Earth Systems*, 12, e2019MS001821, 2020. https://doi.org/10.1029/2019MS001821
Li, Y., Richter, J. H., Chen, C.-C., & Tang, Q.: A strengthened teleconnection of the quasi-biennial oscillation and tropical easterly jet in the past decades in E3SMv1. *Geophysical Research Letters*, 50, e2023GL104517. https://doi.org/10.1029/2023GL104517, 2023.
Lin, S. J., & Rood, R. B.: An explicit Flux-Form Semi-Lagrangian shallow water model on the sphere. Quarterly Journal of the Royal Meteorological Society, 123, 2477–2498.
Lindzen, R. S., and J. R. Holton (1968), A theory of the quasi-biennial oscillation, *J. Atmos. Sci.*, 25, 1095, 1997.
Logan, J. A., M. J. Prather, S. C. Wofsy, and M. B. Mcelroy: Atmospheric Chemistry - Response to Human Influence. Philos T R Soc A, 290, 187-234, 1978.
Lu, B. W., Pandolfo, L., and Hamilton, K.: Nonlinear representation of the quasi-biennial oscillation. *Journal of the atmospheric sciences*, *66*(7), 1886-1904, 2009.
Marquardt, C., & Naujokat, B.: An update of the equatorial QBO and its variability. *World Meteorological Organization-Publications-WMO TD*, *1*, 87-90, 1997.
Maycock, A. C., Randel, W. J., Steiner, A. K., Karpechko, A. Y., Christy, J., Saunders, R., et al.: Revisiting the mystery of recent stratospheric temperature trends, 2018. *Geophysical Research Letters*, 45, 9919–9933. https://doi.org/10.1029/2018GL078035
McFarlane, N. A.: The effect of orographically excited gravity wave drag on the general circulation of the lower stratosphere and troposphere. *Journal of the Atmospheric Sciences*, 44(14), 1775– 1800. https://doi.org/10.1175/1520-0469(1987)044<1775:teooeg>2.0.co;2, 1987.

McLinden, C. A., Olsen, S. C., Hannegan, B., et al.: Stratospheric ozone in 3-D models: A simple chemistry and the cross-tropopause flux, J. Geophys. Res., 105(D11), 14653–14665, doi:10.1029/2000JD900124, 2000.
Mengel, J. G., H. G. Mayr, K. L. Chan, et al.: Equatorial oscillations in the middle atmosphere generated by small-scale gravity waves, Geophys. Res. Lett., 22, 3027-3030, 1995.
Morgenstern, O., Hegglin, M. I., Rozanov, E., et al.: Review of the global models used within phase 1 of the Chemistry–Climate Model Initiative (CCMI), Geosci. Model Dev., 10, 639–671, https://doi.org/10.5194/gmd-10-639-2017, 2017.
Naujokat, B.: An update of the observed quasi-biennial oscillation of the stratospheric winds over the tropics. J. Atmos. Sci., 43, 1873-1877, 1986.
Orbe, C., Plummer, D. A., Waugh, D. W., et al.: Description and Evaluation of the specified-dynamics experiment in the Chemistry-Climate Model Initiative , Atmos. Chem. Phys., 20, 3809–3840, https://doi.org/10.5194/acp-20-3809-2020, 2020.
Park, M., and Coauthors: Variability of stratospheric reactive nitrogen and ozone related to the QBO. J. Geophys. Res. Atmos., 122, 10 103–10 118, https://doi.org/10.1002/2017JD027061, 2017.
Pahlavan, H. A., Fu, Q., Wallace, J. M., & Kiladis, G. N.: Revisiting the quasi-biennial oscillation as seen in ERA5. Part I: Description and momentum budget. *Journal of the Atmospheric Sciences*, *78*(3), 673-691, 2021a.
Pahlavan, H. A., Wallace, J. M., Fu, Q., & Kiladis, G. N.: Revisiting the quasi-biennial oscillation as seen in ERA5. Part II: Evaluation of waves and wave forcing. Journal of the Atmospheric Sciences, 78(3), 693-707, 2021b.
Park, M., Randel, W. J., Kinnison, D. E., et al.: Variability of stratospheric reactive nitrogen and ozone related to the QBO. *Journal of Geophysical Research: Atmospheres*, *122*(18), 10-103, 2017.
Pawson,S., K. Labitzke, R. LenschowB, et al.: Climatology of the Northern Hemisphere stratosphere derived from Berlin analysesp, art 1, Monthly means, technicalr eport, Ser.A ,7(3), Freie Univ. Berlin, 1993.
PhotoComp: Chapter 6 - Stratospheric Chemistry SPARC Report No. 5 on the Evaluation of Chemistry-Climate Models 194-202, 2010.
Plumb, R. A., and R. C. Bell: A model of the quasi-biennial oscillation on an equatorial beta-plane, Q. J. R. Meteorol. Soc., 108, 335-352, 1982.
Prather, J. M., Remsberg, E. E.: The Atmospheric Effects of Stratospheric Aircraft: Report of the 1992 Models and Measurements Workshop. (M.J. Prather, E.E. Remsberg, Eds.), Satellite Beach, FL, 144+268+352 pp, 1993.
Politowicz, P. A., & Hitchman, M. H.: Exploring the effects of forcing quasi-biennial oscillations in a two-dimensional model. *Journal of Geophysical Research: Atmospheres*, *102*(D14), 16481-16497, 1997.
Randall, D. A., Tziperman, E., Branson, M. D., Richter, J. H., & Kang, W. :The QBO-MJO connection: A possible role for the SST and ENSO. *Journal of Climate*, 1-36, 2023.
Randel, W. J., & Cobb, J. B.: Coherent variations of monthly mean total ozone and lower stratospheric temperature. *Journal of Geophysical Research: Atmospheres*, *99*(D3), 5433-5447, 1994.
Randel, W. J., Wu, F., Russell, J. M., Roche, A., & Waters, J. W.: Seasonal cycles and QBO variations in stratospheric CH4 and H2O observed in UARS HALOE data. *Journal of the atmospheric sciences*, *55*(2), 163-185, 1998.

Randel, W. J., and F. Wu: Isolation of the ozone QBO in SAGE II data by singular value decomposition. *J. Atmos. Sci.,***53,** 2546–2559, 1996.
Rasch, P. J., Xie, S., Ma, P.-L., et al.: An overview of the atmospheric component of the Energy Exascale Earth System Model. *Journal of Advances in Modeling Earth Systems*, 11(8), 2377– 2411. https://doi.org/10.1029/2019ms001629, 2019.
Reed, R.: A tentative model of the 26-month oscillation in tropical latitudes. Q. J. R. Meteorol. Soc. 90, 441–466, 1964.
Richter, J. H., Anstey, J. A., Butchart, N., Kawatani, Y., Meehl, G. A., Osprey, S., & Simpson, I. R.: Progress in simulating the quasi-biennial oscillation in CMIP models. *Journal Geophysical Research: Atmospheres*, 125, e2019JD032362. https://doi.org/10.1029/2019JD032362, 2020.
Richter, J. H., Chen, C.-C., Tang, Q., et al.: Improved simulation of the QBO in E3SMv1. *Journal of Advances in Modeling Earth Systems*, 11(11), 3403– 3418. https://doi.org/10.1029/2019MS001763, 2019.
Ruiz, D. J., Prather, M. J., Strahan, S. E., et al.: How atmospheric chemistry and transport drive surface variability of N2O and CFC-11. Journal of Geophysical Research: Atmospheres, 126, e2020JD033979. https://doi.org/10.1029/2020JD033979, (2021).
Ruiz, D. J. and M.J. Prather: From the middle stratosphere to the surface, using nitrous oxide to constrain the stratosphere–troposphere exchange of ozone, Atmos. Chem. Phys., 22, 2079–2093, doi: 10.5194/acp-22-2079-2022, 2022.
Sander, et al. : Chemical kinetics and photochemical data for use in atmospheric studies, evaluation number 15, in JPL Publication 06-2., Jet Propul. Lab., Pasadena, Calif., 2006.
Scaife, A. A., et al. (2014), Predictability of the quasi-biennial oscillation and its northern winter teleconnection on seasonal to decadal timescales, *Geophys. Res. Lett.*, 41, 1752–1758, doi:10.1002/2013GL059160.
Scholz M. and Vigário R.: Nonlinear PCA: a new hierarchical approach, *Proceedings of the 10th European Symposium on Artificial Neural Networks (ESANN)*, pp. 439-444., 2002.
Schwartz, M., Froidevaux, L., Livesey, N., Read, W., and Fuller, R.: MLS/Aura Level 3 Monthly Binned Ozone (O_3) Mixing Ratio on Assorted Grids V005, Greenbelt, MD, USA, Goddard Earth Sciences Data and Information Services Center (GES DISC) [data set], https://disc.gsfc.nasa.gov/datasets/ML3MBO3_005/summary (last access: 30 May 2024), 2021.
Scinocca, J., & Mcfarlane, N.: The parametrization of drag induced by stratified flow over anisotropic orography. Quarterly Journal of the Royal Meteorological Society, 126, 2353–2394. https://doi.org/10.1256/smsqj.56801, 2000.
Shibata, K.: Simulations of Ozone Feedback Effects on the Equatorial Quasi-Biennial Oscillation with a Chemistry–Climate Model. Climate, (9), 123. https://doi.org/10.3390/cli9080123, 2021.
Shuckburgh, E., Norton, W., Iwi, A., & Haynes, P.: Influence of the quasi-biennial oscillation on isentropic transport and mixing in the tropics and subtropics. *Journal of Geophysical Research: Atmospheres*, *106*(D13), 14327-14337, 2001.
Sofieva, V. F., Szelag, M., Tamminen, J., et al.: Updated merged SAGE-CCI-OMPS+ dataset for the evaluation of ozone trends in the stratosphere, Atmos. Meas. Tech., 16, 1881–1899, https://doi.org/10.5194/amt-16-1881-2023, 2023.
Tang, Q., Prather, M. J., Hsu, et al.: Evaluation of the interactive stratospheric ozone (O3v2) module in the E3SM version 1 Earth system model, Geosci. Model Dev., 14, 1219–1236, https://doi.org/10.5194/gmd-14-1219-2021, 2021.

Tang, Q., Golaz, J.-C., Van Roekel, L. P.: The fully coupled regionally refined model of E3SM version 2: overview of the atmosphere, land, and river results, Geosci. Model Dev., 16, 3953–3995, https://doi.org/10.5194/gmd-16-3953-2023, 2023.
Tang, Q., P. G. Hess, B. Brown-Steiner, and D. E. Kinnison : Tropospheric ozone decrease due to the Mount Pinatubo eruption: Reduced stratospheric influx, *Geophys. Res. Lett.*, 40, 5553–5558, doi:10.1002/2013GL056563, 2013.
Tian, W., Chipperfield, M.P., Gray, L.J., Zawodny, J.M.: Quasi-biennial oscillation and tracer distributions in a coupled chemistry-climate model. J. Geophys. Res.: Atmosphere 111 (D20), 2006.
Tilmes, S., Lamarque, J. F., Emmons, L. K., Kinnison, D. E., Ma, P. L., Liu, X., et al.: Description and evaluation of tropospheric chemistry and aerosols in the Community Earth System Model (CESM1.2). Geoscientific Model Development, 8(5), 1395–1426. https://doi.org/10.5194/gmd-8-1395-2015, 2015.
Tilmes, S., Lamarque, J. F., Emmons, L. K., Kinnison, D. E., Marsh, D., Garcia, R. R., et al.: Representation of the Community Earth System Model (CESM1) CAM4-chem within the Chemistry-Climate Model Initiative (CCMI). Geoscientific Model Development, 9(5), 1853–1890. https://doi.org/10.5194/gmd-9-1853-2016, 2016.
Tung, K. K., and H. Yang: Global QBO in circulation and ozone. Part I: Reexamination of observational evidence. *J. Atmos. Sci.,***51,** 2699–2707, 1994.
Tweedy, O. V., Kramarova, N. A., Strahan, S. E., et al., (2017), Response of trace gases to the disrupted 2015–2016 quasi-biennial oscillation, Atmos. Chem. Phys., 17, 6813–6823, 2017.
van der A, R. J., Allaart, M. A. F., and Eskes, H. J.: Extended and refined multi sensor reanalysis of total ozone for the period 1970–2012, Atmos. Meas. Tech., 8, 3021–3035, https://doi.org/10.5194/amt-8-3021-2015, 2015.
Wallace, J., Panetta, R., and Estberg, J.: Representation of the equatorial stratospheric quasibiennial oscillation in EOF phase space, J. Atmos. Sci., 50, 1751–1762, https://doi.org/10.1175/1520-0469(1993)050<1751:ROTESQ>2.0.CO;2, 1993.
Wang L., Hardiman, S. C., Bett, P. E. et al.: What chance of a sudden stratospheric warming in the southern hemisphere?. Environmental Research Letters, 15 (10): 104038. doi:10.1088/1748-9326/aba8c1. ISSN 1748-9326, 2020.
Wang, W., Hong, J., Shangguan, M., et al.: Zonally asymmetric influences of the quasi-biennial oscillation on stratospheric ozone. Atmospheric Chemistry and Physics, 22(20), 13695-13711, 2022.
Watson, P. A. G. and Gray, L. J.: How Does the Quasi-Biennial Oscillation Affect the Stratospheric Polar Vortex?, J. Atmos. Sci., 71, 391–409, https://doi.org/10.1175/JAS-D-13-096.1, 2014.
Xie, F., Zhang, J., Li, X., et al.: Independent and joint influences of eastern Pacific El Niño–southern oscillation and quasi biennial oscillation on Northern Hemispheric stratospheric ozone, Int. J. Climatol., 12, 5289–5307, https://doi.org/10.1002/joc.6519, 2020.
Xie, S., Lin, W., Rasch, P. J., et al.: Understanding cloud and convective characteristics in version 1 of the E3SM Atmosphere Model. Journal of Advances in Modeling Earth Systems, 10(10), 2618– 2644. https://doi.org/10.1029/2018ms001350, 2018.
Zhang, J., Xie, F., Ma, Z., et al.: Seasonal Evolution of the Quasibiennial Oscillation Impact on the Northern Hemisphere Polar Vortex in Winter, J. Geophys. Res., 124, 12568–12586, https://doi.org/10.1029/2019JD030966, 2019.

879 Zhang, J., Xie, F., Ma, Z., Zhang, C., et al.: Seasonal Evolution of the Quasibiennial Oscillation
880 Impact on the Northern Hemisphere Polar Vortex in Winter, J. Geophys. Res., 124, 12568–
881 12586, https://doi.org/10.1029/2019JD030966, 2019.
882 Zhang, R., Tian,W., and Wang, T.: Role of the quasi-biennial oscillation in the downward
883 extension of stratospheric northern annular mode anomalies, Clim. Dynam., 55, 595–612, 2019.
884

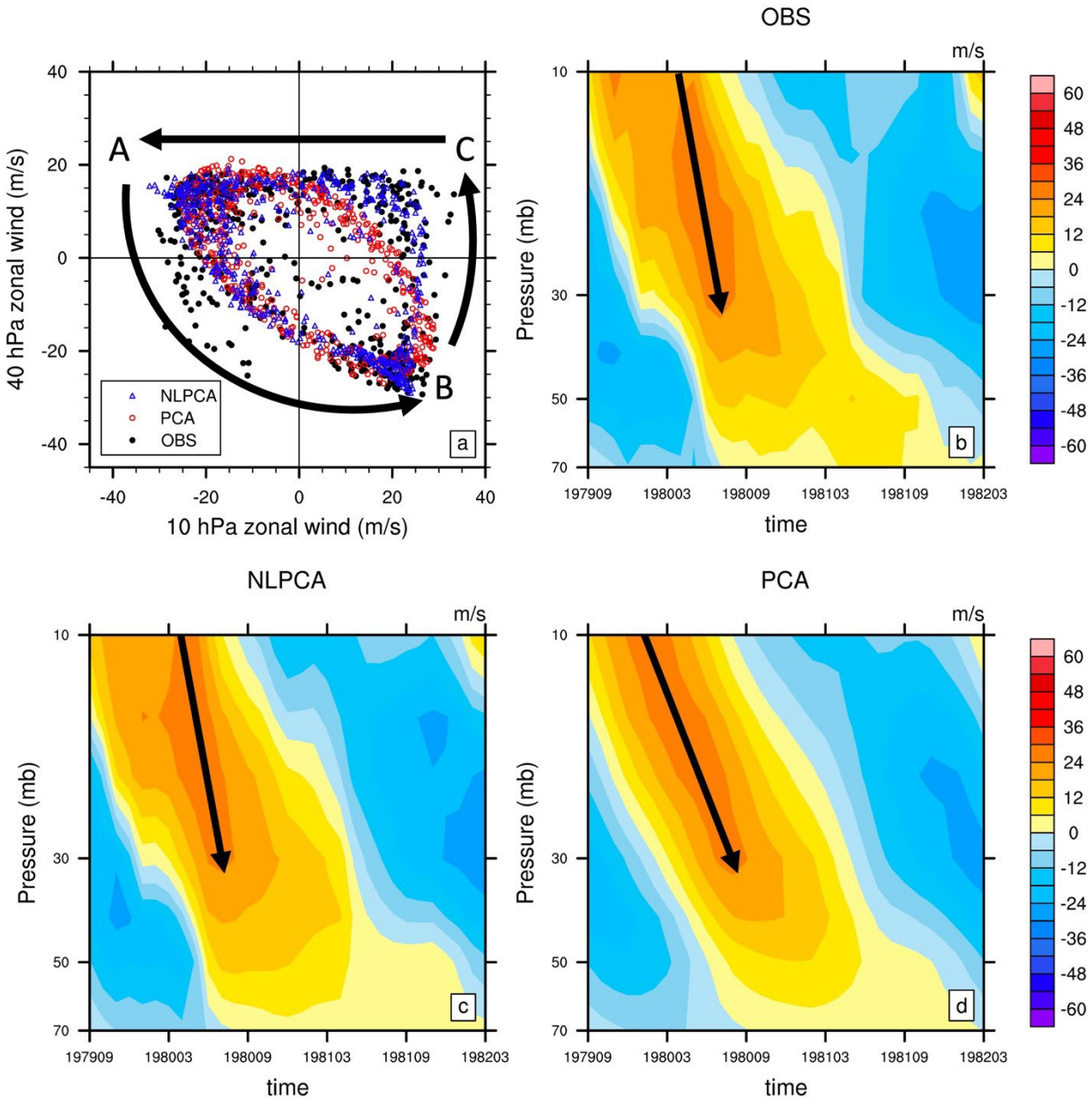

885

886 Fig. 1 (a) Scatter-plot of 1979-2020 anomalous monthly mean zonal wind (m/s) at 10-hPa vs 40-
887 hPa for observation (black), NLPCA reconstruction (blue), and PCA reconstruction (red).
888 Typical cycle of QBO (197909-198203) from (b) Observational station data from University of
889 Berlin, (c) NLPCA reconstruction, (d) PCA reconstruction.

890

891

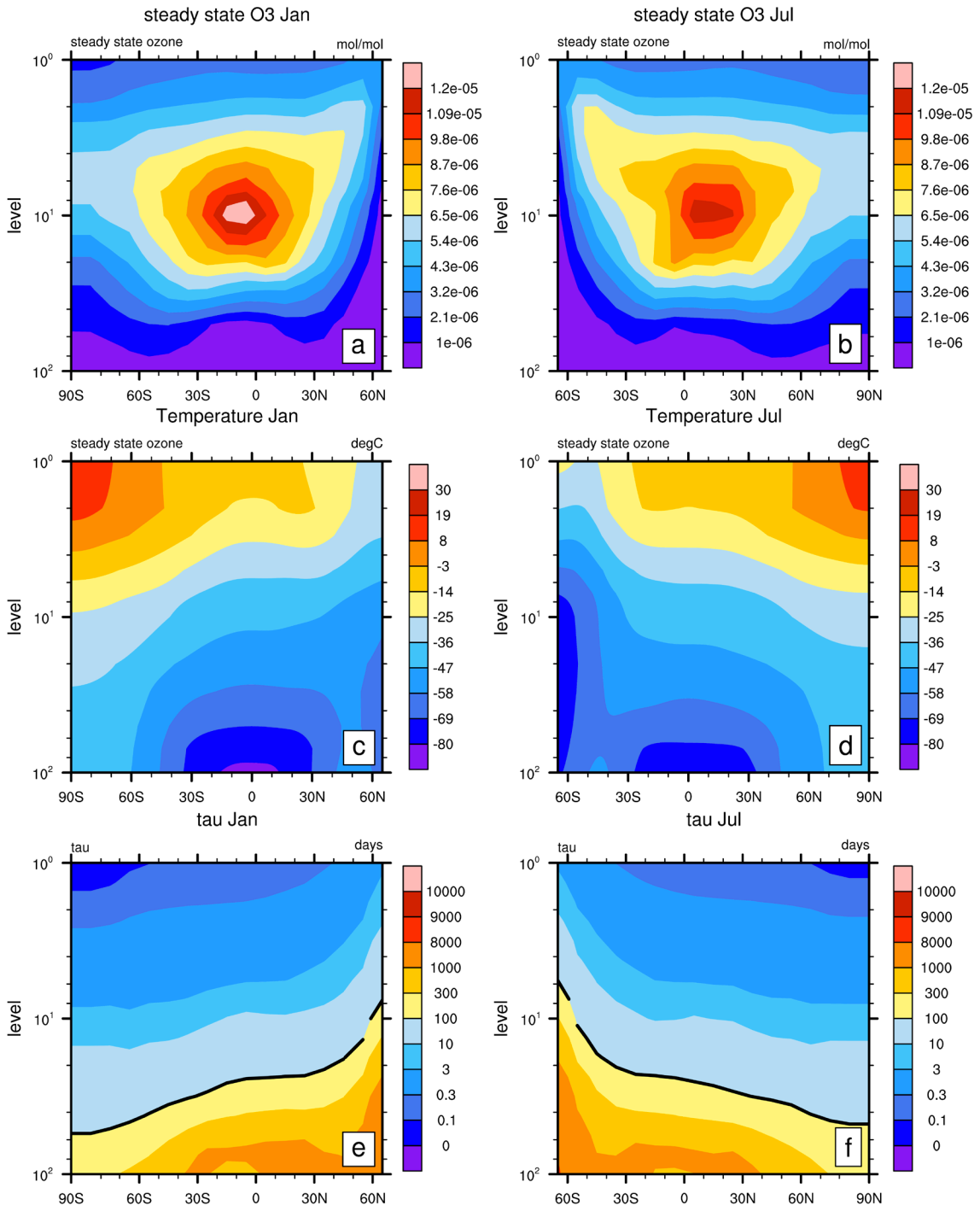

892

893 Fig. 2 The (a, b) steady state ozone (mol/mol) derived using Linoz-v2 on E3SMv2 temperature,

894 (c, d) ERA5 temperature (°C), (e, f) photochemical relaxation time τ (days), and for January and

895 July. The thick black line in (c, d) denotes the 300 value-line.

896

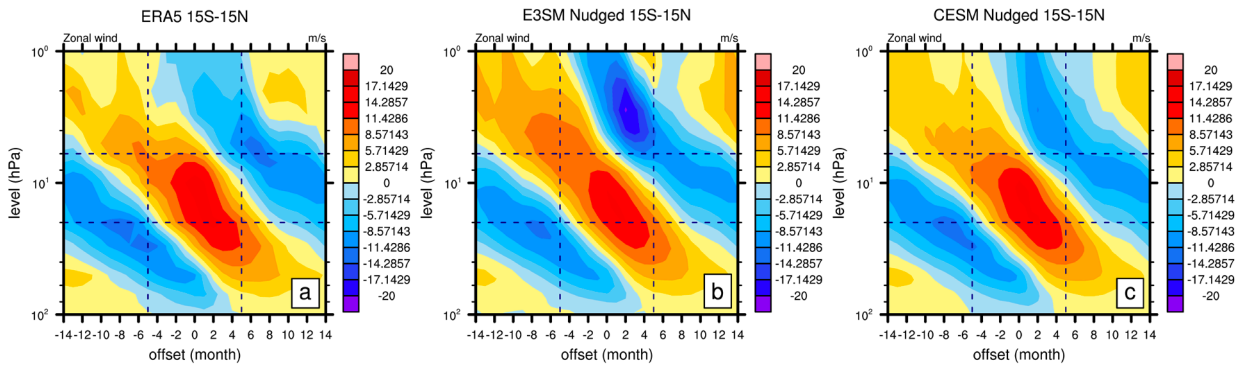

Fig. 3 Pressure-time cross-section of the tropical (15°S-15°N) anomalous zonal wind (m/s) as function of QBO phase for (a, d) ERA5, (b, e) E3SMv2, (c, f) CESM2 for 1979-2020. 0 is centered on the month when QBO index shifts from QBOe to QBOw (determined by when current QBO index<0 and next QBO index>0). The QBO phase is determined by 5S-5N average of the zonal wind.

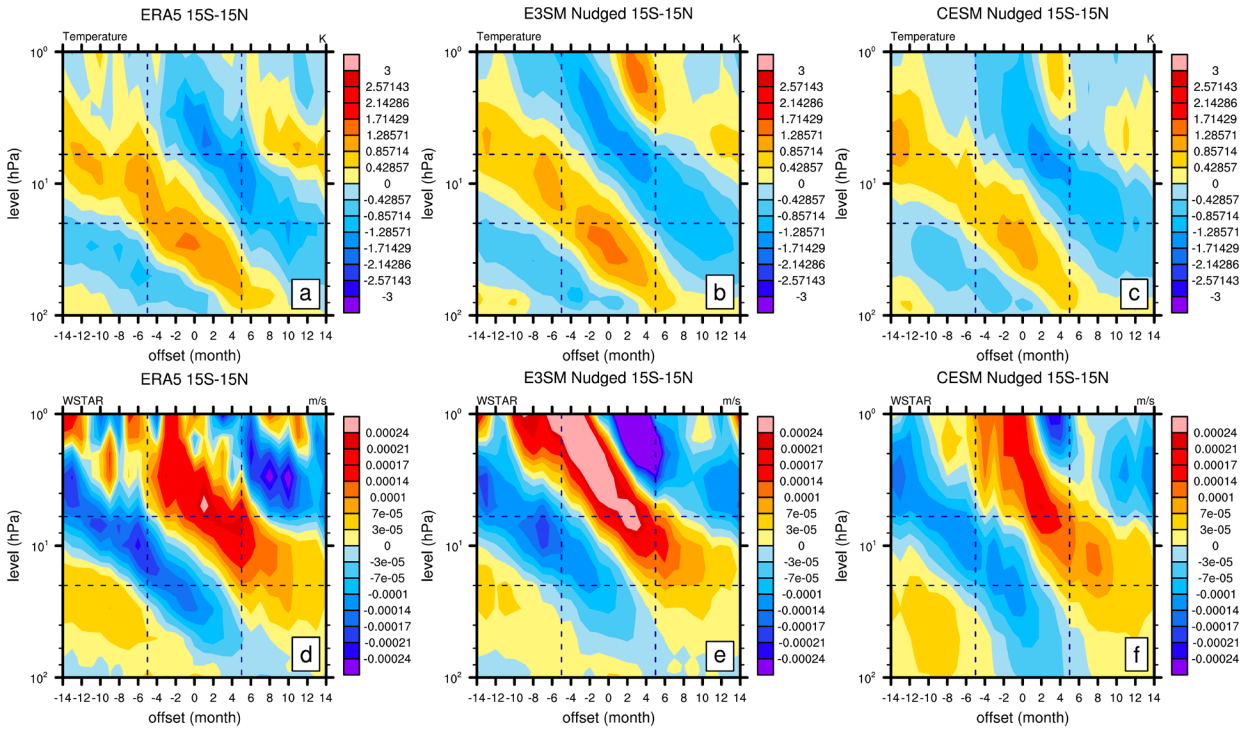

Fig. 4 Pressure-time cross-section of the tropical (15°S-15°N) anomalous temperature (K) and $\underline{w}^*$ (Transformed Eulerian Mean residual vertical transport, m/s) as function of QBO phase for (a, d) ERA5, (b, e) E3SMv2, (c, f) CESM2 for 1979-2020. 0 is centered on the month when QBO index shifts from QBOe to QBOw (determined by when current QBO index<0 and next QBO index>0). The QBO phase is determined by 5S-5N average of the zonal wind.

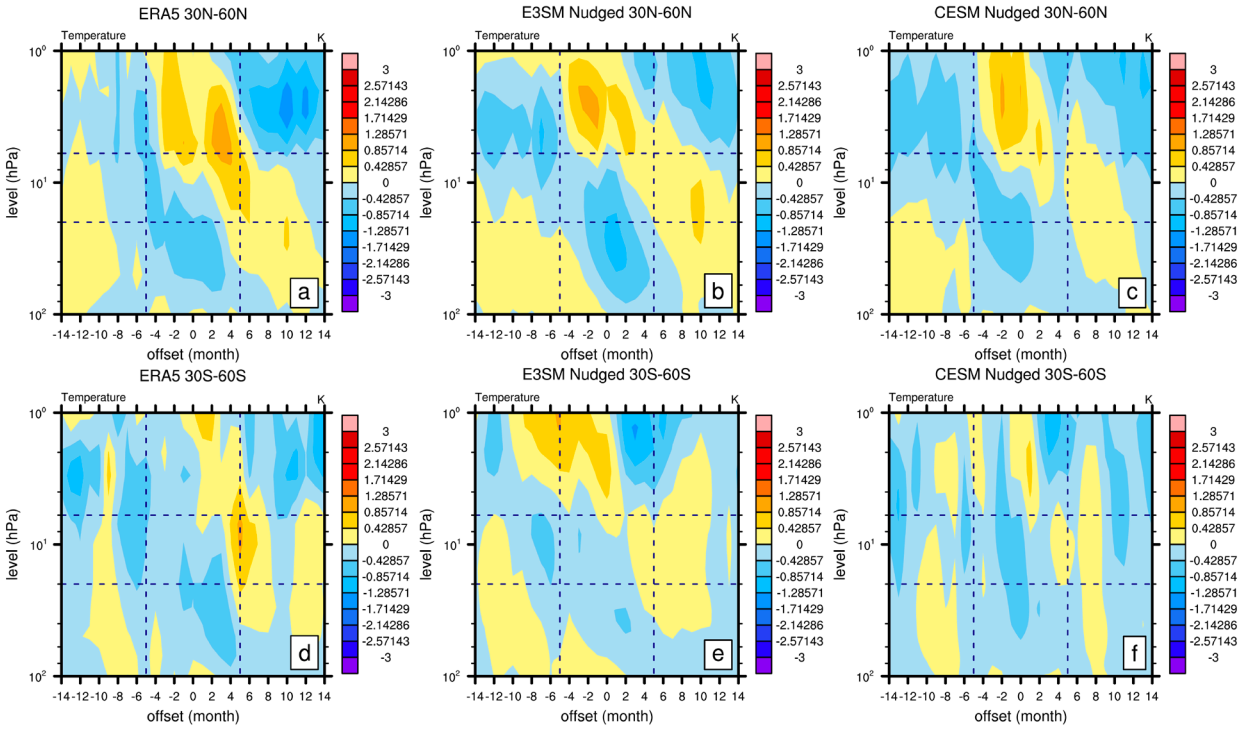

912

913 Fig. 5 Pressure-time cross-section of the extra-tropical (30°N-60°N/30°S-60°S) anomalous
914 temperature (K) as function of QBO phase for (a, d) ERA5, (b, e) E3SMv2, (c, f) CESM2 for
915 1979-2020. 0 is centered on the month when QBO index shifts from QBOe to QBOw
916 (determined by when current QBO index<0 and next QBO index>0). The QBO phase is
917 determined by 5S-5N average of the zonal wind.

918

919

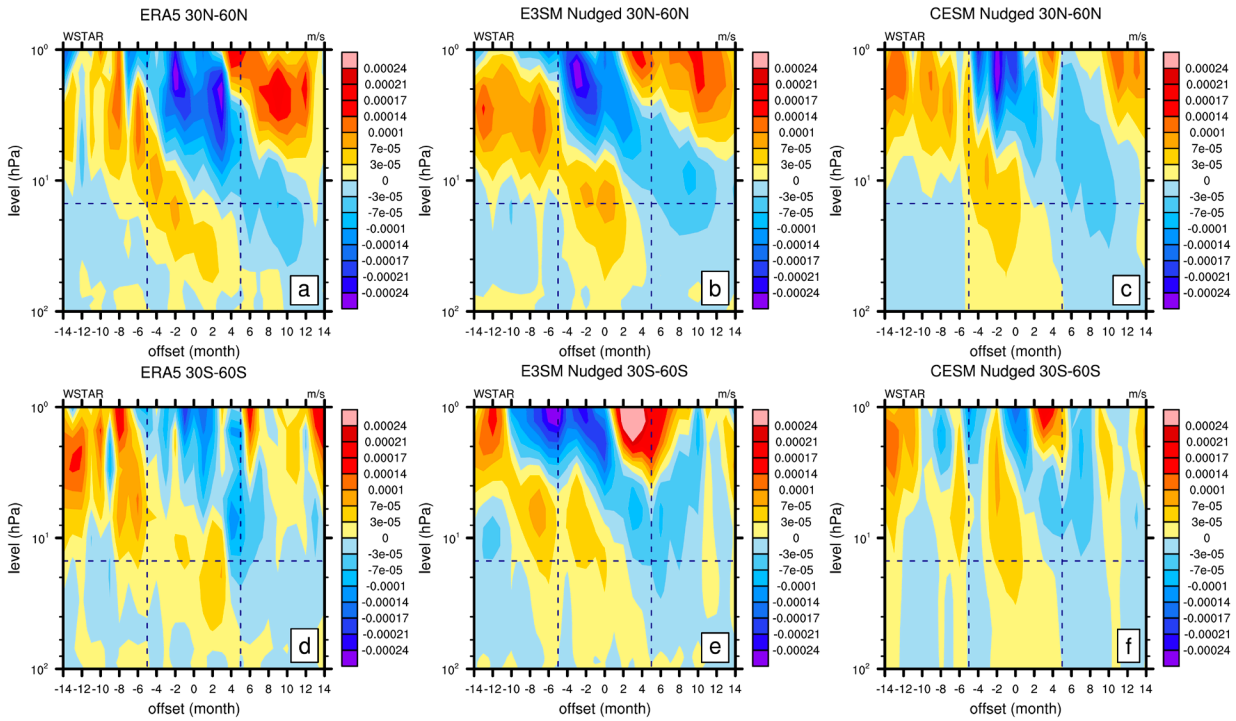

Fig. 6 Pressure-time cross-section of the extratropical (30°N-60°N/30°S-60°S) $\underline{w}^*$ (m/s) as function of QBO for (a, d) ERA5, (b, e) E3SMv2 nudged, (c, f) CESM2 nudged for 1979-2020. 0 is centered on the month when QBO index shifts from QBOe to QBOw (determined by when current QBO index<0 and next QBO index>0). The QBO phase is determined by 5S-5N average of the zonal wind.

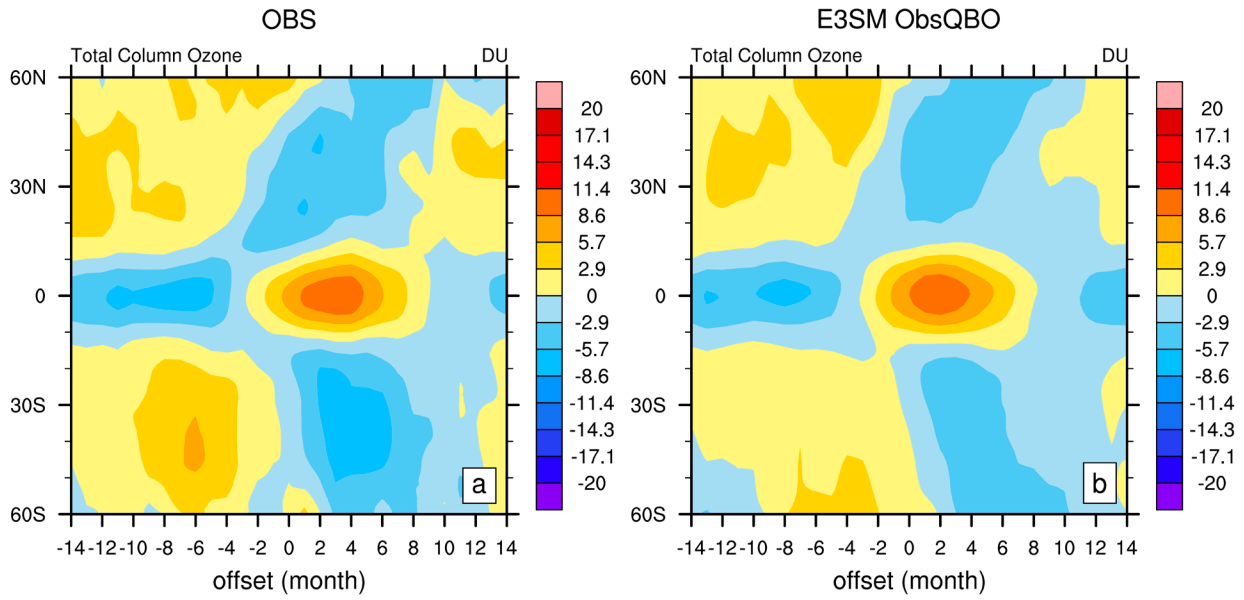

Fig. 7 Total column ozone (TCO, Dobson Unit) anomaly (relative to 1979-2020 mean) composites as function of QBO phase (determined by NLPCA QBO index) for (a) OBS (Multi-Sensor Reanalysis version 2), (b) E3SMv2 nudged simulation for 1979-2020. 0 is centered on the month when QBO index shifts from QBOe to QBOw (determined by when current QBO index<0 and next QBO index>0). The QBO phase is determined by 5S-5N average of the zonal wind.

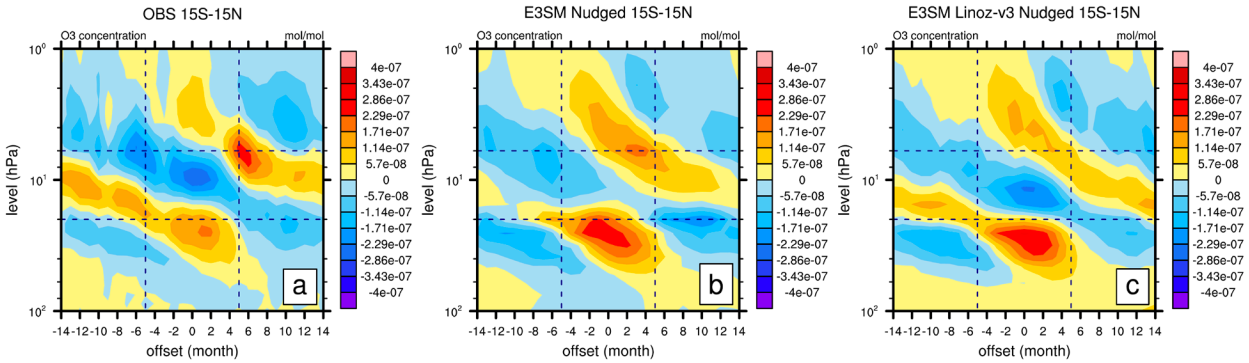

937

938 Fig. 8 Pressure-time cross-section of the tropical (15°S-15°N) anomalous ozone concentration
939 (mol/mol) as function of QBO phase for (a) OBS (Concentration Monthly Zonal Mean), (b)
940 E3SMv2 nudged simulation, (c) E3SMv2 Linoz-v3 nudged simulation for 1979-2020. 0 is
941 centered on the month when QBO index shifts from QBOe to QBOw (determined by when
942 current QBO index<0 and next QBO index>0). The QBO phase is determined by 5S-5N average
943 of the zonal wind. E3SMv2 Linoz-v3 nudged simulation is produced using nudged E3SMv2 with
944 stratospheric chemistry replaced with Linoz-v3.

945

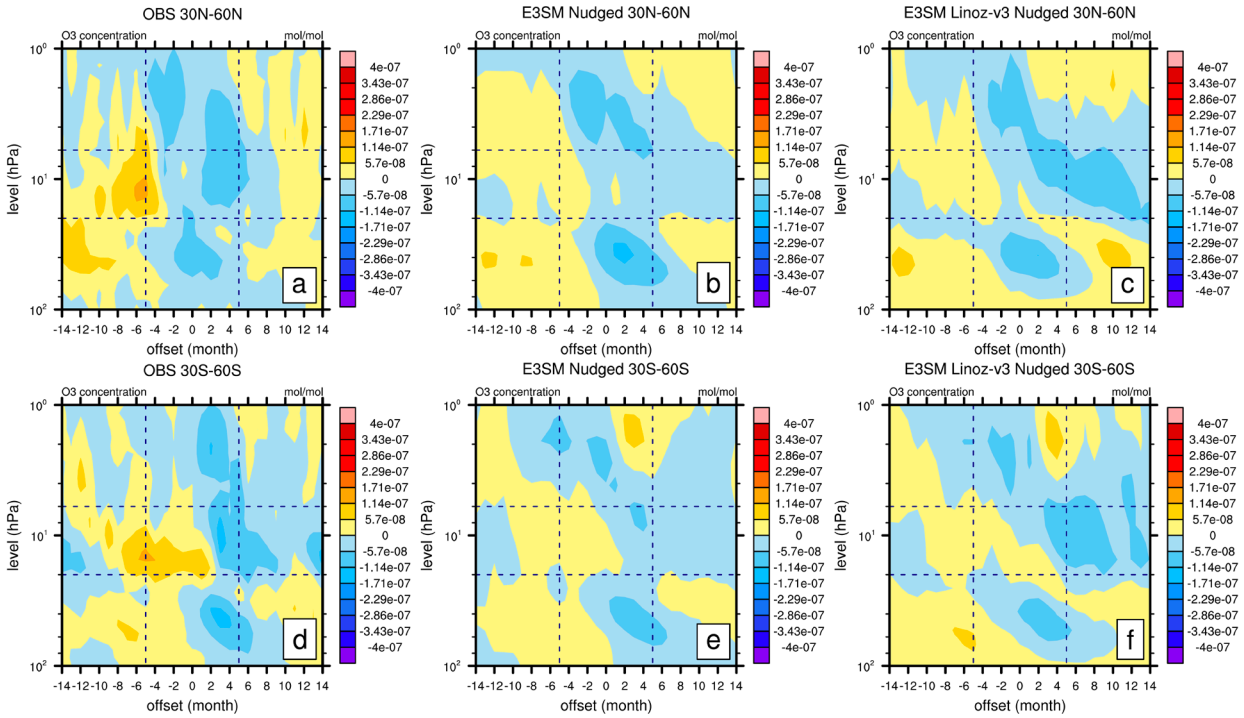

Fig. 9 Pressure-time cross-section of the extratropical (30°N-60°N/30°S-60°S) anomalous ozone concentration (mol/mol) as function of QBO phase for (a, d) OBS (CMZM), (b, e) E3SMv2, (c, f) CESM2 for 1979-2020. 0 is centered on the month when QBO index shifts from QBOe to QBOw (determined by when current QBO index<0 and next QBO index>0). The QBO phase is determined by 5S-5N average of the zonal wind. E3SMv2 Linoz-v3 nudged simulation is produced using nudged E3SMv2 with stratospheric chemistry replaced with Linoz-v3.

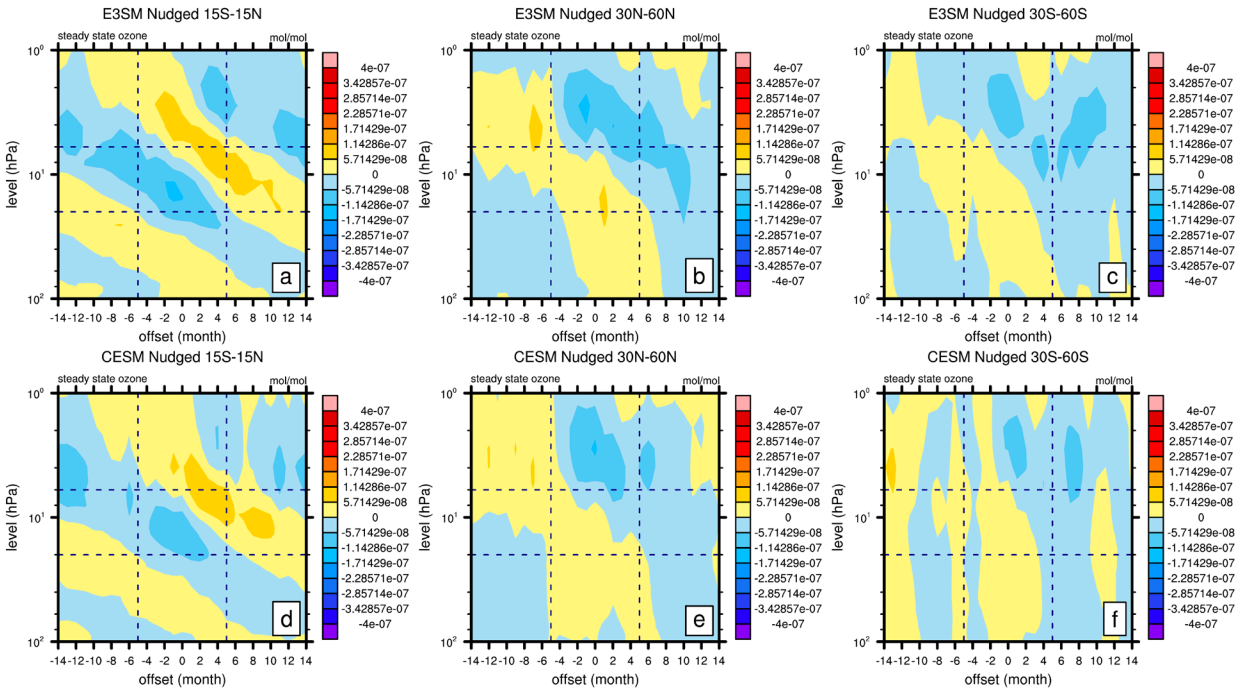

Fig. 10 Pressure-time cross-section of the tropical (15°S-15°N) and extratropical (30°N-60°N/30°S-60°S) anomalous Linoz steady state ozone (mol/mol) as function of QBO phase for (a) E3SMv2 and (b) CESM2 for 1979-2020. 0 is centered on the month when QBO index shifts from QBOe to QBOw (determined by when current QBO index<0 and next QBO index>0). The QBO phase is determined by 5S-5N average of the zonal wind.

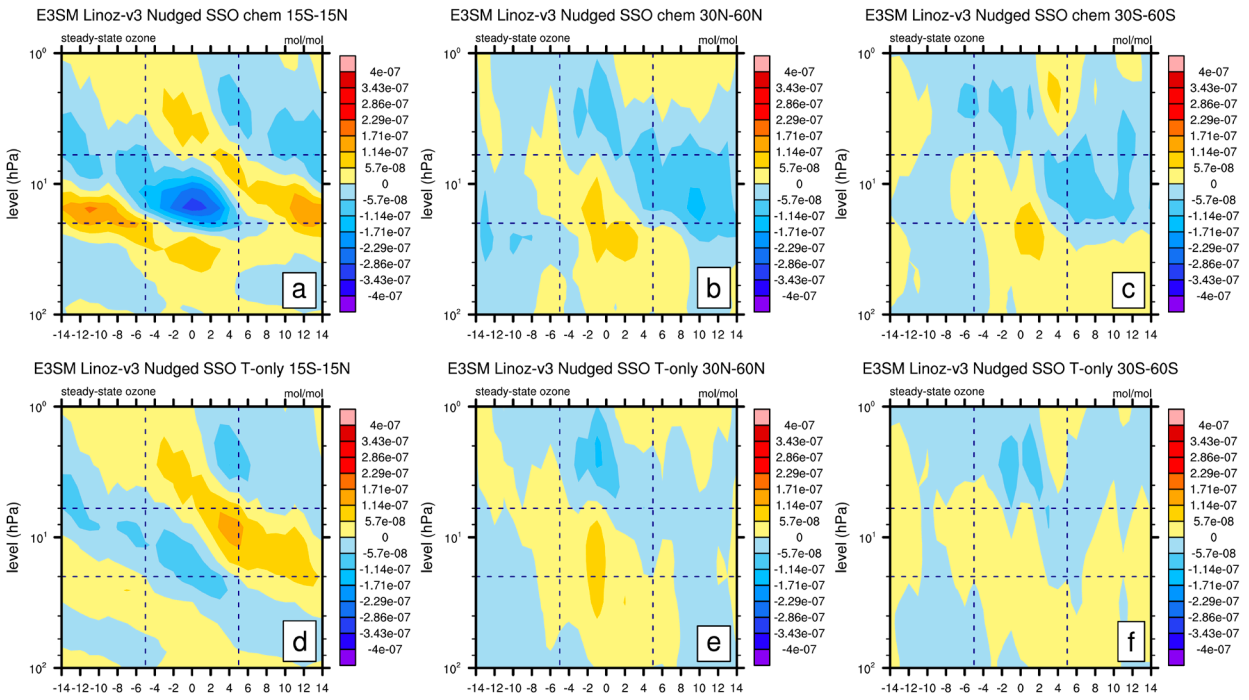

Fig. 11 Pressure-time cross-section of the tropical (15°S-15°N) and extratropical (30°N-60°N/30°S-60°S) steady state ozone (mol/mol) as function of QBO for E3SMv2 Linoz-v3 Nudged simulation using (a, b, c) Linoz-v3 chemistry (NO_y-N_2O-CH_4-H_2O), (d, e, f) temperature only for 1979-2020. 0 is centered on the month when QBO index shifts from QBOe to QBOw (determined by when current QBO index<0 and next QBO index>0). The QBO phase is determined by 5S-5N average of the zonal wind.

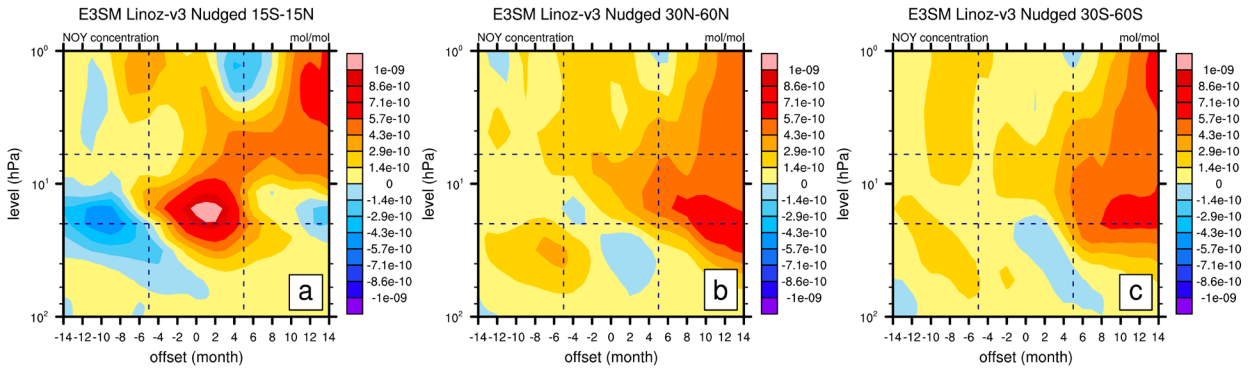

970

971 Fig. 12 Pressure-time cross-section of the tropical (15°S-15°N) and extratropical (30°N-
972 60°N/30°S-60°S) NO_y (mol/mol) as function of QBO (a, b, c) E3SMv2 Linoz-v3 for 1979-2020.
973 0 is centered on the month when QBO index shifts from QBOe to QBOw (determined by when
974 current QBO index<0 and next QBO index>0). The QBO phase is determined by 5S-5N average
975 of the zonal wind.

976

977

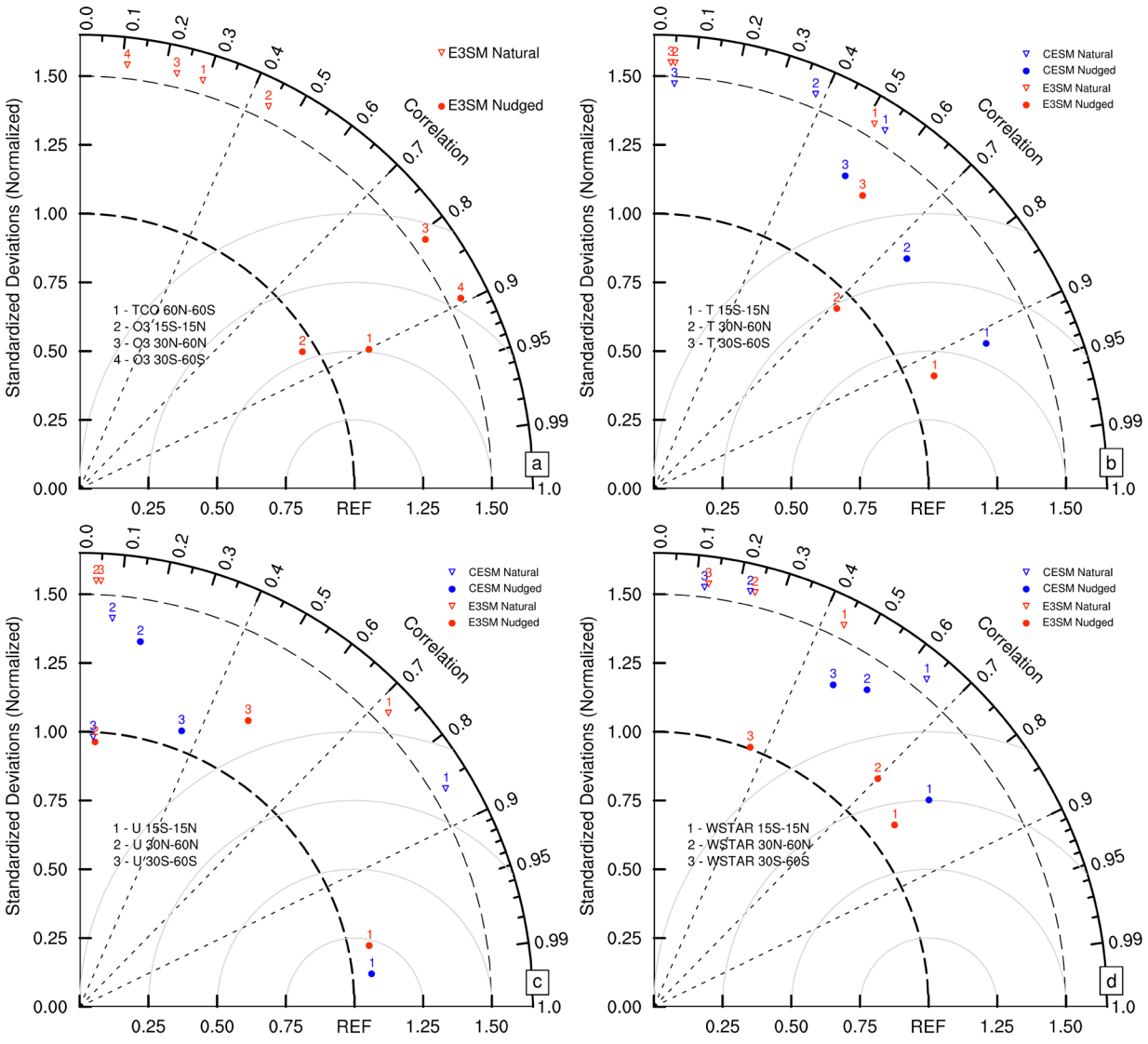

Fig. 13 Taylor diagram of the E3SMv2/CESM2 simulation for various datasets for 1979-2020. (a) The area-weighted total column ozone (60°S-60°N, DU) and pressure-time cross-sections of ozone concentration (15°S-15°N, 30°N-60°N, 30°S-60°S, mol/mol) anomalies with OBS (MSR and CMZM), respectively. (b) The area-weighted pressure-time cross-sections of temperature (15°S-15°N, 30°N-60°N, 30°S-60°S, K) anomalies with ERA5. (c) The area-weighted pressure-time cross-sections of zonal wind (15°S-15°N, 30°N-60°N, 30°S-60°S, m/s) anomalies with ERA5. For pattern correlations, the cross-sections are weighted by pressure layer thickness. On all Taylor diagrams, the model standard deviations are normalized by dividing the standard deviations of the reference.